HHS Public Access

Author manuscript

Nat Neurosci. Author manuscript; available in PMC 2021 February 03.

Published in final edited form as:

Nat Neurosci. 2020 October ; 23(10): 1253–1266. doi:10.1038/s41593-020-0684-9.

High fat food biases hypothalamic and mesolimbic expression of consummatory drives

Christopher M. Mazzone[1,9], **Jing Liang-Guallpa**[2,3,4,9], **Chia Li**[2,3], **Nora S. Wolcott**[2], **Montana H. Boone**[2], **Morgan Southern**[2], **Nicholas P. Kobzar**[1], **Isabel de Araujo Salgado**[2,3], **Deepa M. Reddy**[2], **Fangmiao Sun**[5,6,7,8], **Yajun Zhang**[5,6,7,8], **Yulong Li**[5,6,7,8], **Guohong Cui**[1,*], **Michael J. Krashes**[2,3,*]

[1]*In Vivo* Neurobiology Group, Neurobiology Laboratory, National Institute of Environmental Health Sciences (NIEHS), National Institutes of Health, Research Triangle Park, NC 27709, USA

[2]Diabetes, Endocrinology, and Obesity Branch, National Institute of Diabetes and Digestive and Kidney Diseases (NIDDK), National Institutes of Health, Bethesda, MD 20892, USA

[3]National Institute on Drug Abuse (NIDA), National Institutes of Health, Baltimore, MD 21224, USA

[4]NIH-Brown University Graduate Program in Neuroscience, Bethesda, MD 20892, USA

[5]State Key Laboratory of Membrane Biology, Peking University School of Life Sciences, Beijing 100871, China

[6]PKU-IDG/McGovern Institute for Brain Research, Beijing 100871, China

[7]Peking-Tsinghua Center for Life Sciences, Academy for Advanced Interdisciplinary Studies, Peking University, Beijing 100871, China

[8]Chinese Institute for Brain Research, Beijing 100871, China

[9]These authors contributed equally

Summary

Maintaining healthy body weight is increasingly difficult in our obesogenic environment. Dieting efforts are often overpowered by the internal drive to consume energy-dense foods. While the selection of calorically-rich substrates over healthier options is identifiable across species, the

* cuig@mail.nih.gov; michael.krashes@nih.gov.

Author contributions C.M.M., J. L.-G., and M.J.K. designed experiments with technical input from G.C., J. L.-G., N.S.W., M.H.B., and M.S. performed and analyzed home cage consumption and body composition, fast-refeed, and optogenetic experiments. C.M.M. performed and analyzed home cage AgRP fiber photometry experiments and DA sensor experiments. C.L. performed and analyzed LepR-Cre fiber photometry experiments. C.L. and I.D.A.S. performed electrophysiology recordings. J. L.-G. performed and analyzed gastric infusion and VTA studies. F.S., Y.Z., and Y.L. provided the DA2m sensor and provided technical guidance. N.P.K. and D.M.R. performed histological verification and imaging. C.M.M., J. L.-G., and M.J.K wrote the manuscript with input from G.C., C.L., I.D.A.S., N.S.W., M.H.B., M.S., N.P.K., D.M.R., F.S, Y.Z., and Y.L.

Competing interests The authors declare no conflicts of interest.

Data availability Data and supporting materials will be made available by the corresponding authors upon request.

Code availability Code is available by the corresponding authors upon request or directly at https://www.niehs.nih.gov/research/atniehs/labs/ln/pi/iv/tools/index.cfm

mechanisms behind this choice remain poorly understood. Using a passive devaluation paradigm, we found that exposure to high-fat diet (HFD) suppresses the intake of nutritionally-balanced standard chow diet (SD) irrespective of age, sex, body mass accrual and functional leptin or melanocortin-4 receptor signaling. Longitudinal recordings revealed this SD devaluation and subsequent shift toward HFD consumption is encoded at the level of hypothalamic Agouti-related peptide (AgRP) neurons and mesolimbic dopamine signaling. Prior HFD consumption vastly diminished the capacity of SD to alleviate the negative valence associated with hunger and the rewarding properties of food discovery even after periods of HFD abstinence. These data reveal a neural basis behind the hardships of dieting.

Our brains are tuned to prefer and consume energy-rich foods, such as those high in fats, as an evolutionary mechanism for survival and maturation. However, exposure to these diets can result in overconsumption of calories, leading to obesity and numerous health complications[1,2]. The drive to eat high-fat foods is exacerbated by the subsequent devaluation of less palatable, nutritionally-balanced diets. A major gap in our knowledge stems from our lack of understanding of how this devaluation occurs. Thus, recognizing how brain activity adapts to discrete diets during periods of food exposure and withdrawal, as well as accompanying weight changes, is critical to our ability to develop targeted therapeutics.

Several neural circuits govern the drive to eat for both homeostatic energy needs and the rewarding properties of food[3]. Interoceptive Agouti-related peptide (AgRP)-expressing neurons of the hypothalamic arcuate nucleus (ARC) are required for feeding and drive food intake when activated[4–7]. These neurons respond to food presentation, sensory cues of food, and direct macronutrient infusion to the gut[8–11]. In line with the unpleasant sensations associated with energy deficit reported in humans, ARC^{AgRP} neurons broadcast a negative valence state in the absence of food[12]. Caloric deprivation/dieting exacerbates this adverse condition, resulting in food seeking to dull this signal. It is suggested that high-fat diet (HFD) access enhances ARC^{AgRP} activity and may represent a mechanism promoting sustained overconsumption; however, these experiments were carried out in isolated brain slices[13].

Reinforcing dopamine (DA) neurons of the ventral tegmental area (VTA) have been shown to encode the palatability and salience of reward[14–16]. Although ARC^{AgRP} activity can potentiate DA release in response to food, ARC^{AgRP} neurons are not required for consumption of palatable diets[17,18]. While studies have demonstrated changes in hypothalamic and mesolimbic basal activity after palatable diet exposure[19–25], the endogenous dynamics and function of ARC^{AgRP} neurons and DA signaling in response to a devalued standard chow diet (SD) remain to be explored. Furthermore, the long-term effects of HFD on these putative activity modifications following HFD withdrawal have yet to be elucidated.

Given that foods with higher fat content are overconsumed and rated as more palatable than lower-calorie foods[26], we hypothesized that HFD exposure would rapidly rewire canonical homeostatic and hedonic nodes in the brain that act to relay incoming caloric information and direct consumption. We employed a multidisciplinary approach to model and study the

passive devaluation of a SD in mice following HFD challenge and withdrawal. Our findings reveal that mice forego SD consumption following access to HFD, even in states of caloric deprivation, and that this motivational drive is reflected by altered responses of ARC^{AgRP}, VTA^{DA} neurons and accumbal DA release to food. Following HFD exposure, SD is no longer capable of fully suppressing the deleterious affective state of hunger at the level of ARC^{AgRP} neurons or amplifying the appetitive nature of food discovery through mesolimbic DA signaling. These findings reveal how simultaneous preference for HFD and devaluation of SD give rise to overeating and how perturbation of these circuits underlie the familiar complications of dieting.

Results

High fat diet-induced weight gain and preference

To determine how HFD access affects food intake, body composition and potential HFD-evoked devaluation of a SD, we split adult male and female wildtype C57BL/6J mice into two groups (Fig. 1a). Both began with *ad libitum* access to SD (baseline period). One group remained on SD for the duration of the study. The other was supplied *ad libitum* access to both SD and a 60% HFD for 8 weeks (experimental period), followed by HFD removal for two weeks (withdrawal period). While both groups started with similar weights and daily SD calories consumed, only the HFD-fed mice increased body weight, fat mass, and total daily calories consumed without affecting lean mass (Fig. 1b–c, Extended Data Fig. 1a–c, for full statistical results see Supplementary Table 1). HFD exposed mice exhibited an immediate preference for the HFD in lieu of SD (Fig. 1d, Extended Data Fig. 1d). As previously reported, genetically identical mice exhibited a wide range of body-weight changes due to HFD exposure (Extended Data Fig. 1c)[27]. Importantly, every mouse exposed to HFD showed a marked reduction of SD intake and there was no correlation between the average amount of SD consumed during the experimental period and total body weight change after the experimental period (Extended Data Fig. 1d–e). Removal of HFD resulted in precipitous weight loss due to the failure of mice to consume the required daily calories from SD[28], thus emphasizing a potential HFD-induced devaluation of SD to the point of self-restricted caloric deprivation (Fig. 1b–d). Body weight, fat mass levels and daily calories consumed did not recover to SD control values even after two weeks of HFD withdrawal, indicating prolonged physiological adaptations following HFD challenge (Fig. 1b–d, Extended Data Fig. 1a)[28].

Devaluation of SD during periods of hunger

To assess if HFD exposure changes the valuation and subsequent consumption of SD during periods of physiological hunger, we food deprived a separate cohort of mixed-sex, adult mice overnight, then measured SD consumption over a one-hour refeeding session (Fig. 1e). We longitudinally tested fast-refeed SD consumption in mice before access to HFD (baseline), at 1, 4, and 8 weeks during home cage HFD access, and after 2 weeks of HFD withdrawal (Fig. 1e). As a control, mice maintained on *ad libitum* SD were tested in parallel. Mice maintained strictly on SD showed consistent SD caloric intake across the experimental time course, while HFD exposed mice exhibited a stark reduction in SD intake during the refeeding sessions both compared to their response at baseline (Fig. 1f) and to the SD group

at each time point (Extended Data Fig. 1f). This passive devaluation remained intact, although to a lesser degree, during the withdrawal period (Fig. 1f; Extended Data Fig. 1f). Critically, the SD devaluation across sessions did not correlate with changes in body weight across the experiment (Extended Data Fig. 1g). To further uncouple changes in body weight from SD devaluation after HFD exposure, a new cohort of animals including a group of HFD-fed animals yoked to match the weights of the *ad libitum* SD group displayed a similar devaluation of SD following a fast-refeed, although this returned to baseline levels 2 weeks after HFD withdrawal (Extended Data Fig. 1h–j). To ensure HFD challenged animals were still motivated to eat, we repeated the fast-refeed test sessions with access to both SD and HFD after fasting (Fig. 1g). During the experimental period, mice exposed to HFD robustly consumed HFD to greater caloric values than baseline consumption of SD while minimally consuming SD (Fig. 1h, Extended Data Fig. 1k). Interestingly, the amount of HFD calories consumed during the one-hour refeeding period diminished the longer animals were exposed to HFD (Extended Data Fig. 1k). In agreement with intermittent binge models, consumption of HFD during a fast-refeed session was further pronounced following HFD withdrawal (Fig. 1h, Extended Data Fig. 1k)[29].

Our data demonstrate that lean animals exposed to HFD show devaluation toward SD and this occurred independent of weight gain (Extended Data Fig. 1g–j). To test this model in hyperphagic, genetically obese animals and determine the functional contribution of two classic satiety signaling pathways, we repeated the experimental design using two mouse models of obesity: those lacking the melanocortin 4 receptor (Mc4r KO) and those incapable of producing leptin (Leptin KO; Extended Data Fig. 2a,d)[30,31]. Despite being obese from the start of the experiment, HFD-fed Mc4r KO and Leptin KO mice exhibited comparable devaluation of SD during a fast-refeed period compared to their heterozygous littermate controls (Extended Data Fig. 2a–f).

In the experiments above, the earliest time point tested was 1 week following HFD access when body weights on average began deviating and metabolic changes have been reported[32]. To determine if HFD alters fasting-induced feeding of SD prior to metabolic changes, we repeated the experiment in mice subjected to HFD for only 24 hours (Extended Data Fig. 2g). Following overnight food deprivation, mice provided HFD for 24 hours showed reduced SD intake compared to baseline measurements and littermate, HFD-naive control mice (Extended Data Fig. 2h–i). Collectively, these results demonstrate that HFD exposure rapidly, profoundly, and lastingly reduces SD intake in varying physiological conditions, independent of sex, diet-induced body weight changes, functional Mc4r or leptin signaling, or pre-existing obesity.

Modified hypothalamic responses to SD after HFD exposure

The sensory detection and subsequent consumption of food rapidly suppresses ARC^{AgRP} activity, serving to silence the negative valence associated with hunger[8,9,12]. To determine how HFD exposure impacts ARC^{AgRP} responses to food, we longitudinally recorded ARC^{AgRP} population activity using the fluorescent calcium sensor GCaMP6s[33] as both male and female mice transitioned to and from HFD (Fig. 2a–b). GCaMP6s-expressing mice were maintained on SD and underwent two baseline recordings in both the fed and fasted

conditions before half of the mice were supplied HFD using the timeline described (Fig. 2b). At baseline, all mice were provided a SD pellet (Pellet 1) to their home cage while recording ARC^{AgRP} activity. Five minutes later, a second SD pellet (Pellet 2) was added for an additional five minutes (Fig. 2b). Once the HFD group was exposed to HFD, the second pellet (Pellet 2) during recording sessions was a HFD pellet for this group only (Fig. 2b).

During both baseline recordings, we observed robust inhibition of ARC^{AgRP} neurons by SD Pellet 1 presentation in all fasted animals; this was accompanied by comparable SD intake in each session (Fig. 2c–f, Extended Data Fig. 3a–b). Whereas this response to SD Pellet 1 was consistent across time in mice maintained on SD, those provided with HFD had significantly reduced population responses to SD Pellet 1 compared to both their baseline response and to control mice maintained on SD (Fig. 2c–f, Extended Data Fig. 3a–b). While this attenuated ARC^{AgRP} response to SD Pellet 1 corresponded with a reduction in the amount of SD consumed during the 5 min window (Fig. 2e–f, Extended Data Fig. 3a–b), ARC^{AgRP} inhibition was blunted prior to food intake in the HFD-exposed animals (Fig. 2j–k). Importantly, this sensory-evoked ARC^{AgRP} inhibition to SD preceding consumption remained constant in HFD-naïve animals (Fig 2i,k). Remarkably, diminished ARC^{AgRP} inhibition to SD Pellet 1 was still present following a 2-week withdrawal from HFD, akin to a strict diet, emphasizing the enduring effect HFD-exposure has on this signaling system (Fig. 2d–f, Extended Data Fig. 3a–b). Furthermore, the change in ARC^{AgRP} dynamics in response to SD Pellet 1 were largely independent of body weight change throughout the experiment (Extended Data Fig. 3c–f). In summary, while SD Pellet 1 presentation stably reduced ARC^{AgRP} activity in HFD-naïve mice, it was no longer capable of silencing the negative affective state linked to hunger (encoded by ARC^{AgRP} neurons) after HFD challenge. These results provide a potential neural mechanism for why SDs lose their capacity to curb hunger after prior access to palatable foods.

The addition of a second SD Pellet 2 did not further inhibit ARC^{AgRP} activity in SD mice (Fig. 2c,g); however, presentation of a HFD Pellet 2 promoted additional inhibition of ARC^{AgRP} neurons in HFD exposed mice (Fig. 2d,g, Extended Data Fig. 3g). Therefore, the diminished response to SD Pellet 1 in HFD-challenged mice was not due to a floor effect or impairment of ARC^{AgRP} activity, but a preference for HFD as evidenced by total food consumption during this window (Fig. 2h, Extended Data Fig. 3h).

To determine how rapidly this devaluation of SD and proclivity for HFD consumption occurs in ARC^{AgRP} neurons, we repeated this experiment with mice provided access to HFD for only 24 hours (Extended Data Fig. 3i). At baseline, prior to HFD exposure, all mice displayed a robust inhibition of ARC^{AgRP} activity in response to SD Pellet 1 and this effect remained constant after addition of SD Pellet 2 (Extended Data Fig. 3j–n). However, just 24 hours of homecage HFD exposure led to a significant reduction of ARC^{AgRP} inhibition and intake of SD Pellet 1 (Extended Data Fig. 3j–l). HFD Pellet 2 presentation reversed this blunted ARC^{AgRP} inhibition in all HFD-exposed mice corresponding to increased calories consumed (Extended Data Fig. 3j,m–n). Thus, we observed a similar short- and long-term devaluation of SD in HFD-challenged mice.

There were minimal changes in ARC^{AgRP} activity upon introduction of SD Pellet 1 across all conditions and time points under fed (sated) conditions, corresponding to nominal chow consumption (Extended Data Fig. 4a–g). While the addition of SD Pellet 2 failed to alter ARC^{AgRP} activity over time in HFD-naïve mice, presentation of HFD Pellet 2 to the HFD-exposed group significantly suppressed ARC^{AgRP} activity 1 week into HFD challenge when the diet was still relatively new (Extended Data Fig. 4b–c, h–i). This response dissipated at 4 and 8 weeks, only to reemerge following a 2-week HFD withdrawal (Extended Data Fig. 4c, h–i). Thus, consumption of HFD under satiation acts to further suppress the negative valence signal associated with these cells,[12] an effect potentiated after HFD restriction. Collectively, these observations provide a plausible neural process behind the tendency to consume energy dense foods in the calorically replete state.

A prior study indicated that HFD-induced obesity altered the intrinsic properties of ARC^{AgRP} neurons by increasing firing rate and resting membrane potential[13]. Although we observed a similar phenomenon in isolated brain slices (data not shown), these between-group studies were performed devoid of neural input. Here, using spectrum-based, longitudinal fiber photometry recordings, we were able to capture the putative changes of ARC^{AgRP} basal activity following HFD exposure (Extended Data Fig. 5a). HFD access reduced resting ARC^{AgRP} activity relative to the SD group in both the fed and fasted states (Extended Data Fig. 5b). Despite this robust decline in basal activity, fasting increased observed GCaMP fluorescence by ~50% relative to the sated state, suggesting similar magnitudes of fasting-induced enhancements of ARC^{AgRP} activity regardless of HFD history (Extended Data Fig. 5c). Counter to ex vivo slice experiments, these findings demonstrate that HFD challenge, comparable to the acute effects of alcohol and non-nutritive drugs[17], negatively shifts basal ARC^{AgRP} activity during HFD exposure.

ARC^{AgRP} neurons receive dense GABAergic input from leptin receptor (LepR)-expressing neurons in the dorsomedial hypothalamus (DMH) that have opposing responses to food[34]. To ascertain whether similar HFD-induced alterations occurred in this upstream circuit, we took a two-pronged approach and measured the impact of HFD challenge on both the synaptic plasticity of this $DMH^{LepR} \rightarrow ARC^{AgRP}$ connection and the *in vivo* DMH^{LepR} population dynamics in response to food. Channelrhodopsin-2 (ChR2) was targeted to DMH^{LepR} neurons and light-evoked, paired pulse experiments were performed in $ARC^{Npy/AgRP}$ neurons (Figure 3a–b). Importantly, 98% of AgRP neurons co-express NPY[35]. Chronic HFD significantly increased the paired pulse ratio of light-evoked postsynaptic inhibitory currents from DMH^{LepR} neurons onto ARC^{AgRP} neurons, reflecting a reduced probability of GABAergic release from these synapses (Figure 3b). While this input likely does not reflect the source of HFD-induced decreases in basal ARC^{AgRP} activity revealed in our photometry recordings, it nonetheless emphasizes larger scale intrahypothalamic circuit dynamics influenced by HFD.

To assess how this intrahypothalamic input may contribute to altered ARC^{AgRP} responses to food, we selectively expressed GCaMP6s in DMH^{LepR} neurons, thus providing longitudinal access to activity dynamics to food presentation before, during and after HFD challenge in both the fasted and fed conditions (Figure 3c–d). We found that HFD exposure significantly dampened the baseline DMH^{LepR} population response to and consumption of SD Pellet 1 in

hungry mice, an effect still present after HFD withdrawal (Figure 3e–g). While presentation of SD Pellet 2 in hungry HFD-naïve mice increased activity, this was strongly amplified by the introduction of HFD Pellet 2 following home cage HFD exposure, resulting in higher caloric intake (Figure 3e–g). Food intake and activity changes to SD Pellet 1 were minimal in the fed condition (Figure 3h–j). However, we found that addition of HFD Pellet 2 in fed mice significantly altered DMH^{LepR} activity 1 week after HFD exposure and this effect was further heightened following HFD-withdrawal when intake was high (Figure 3h–j). A reduction in GABAergic transmission from $DMH^{LepR} \rightarrow ARC^{AgRP}$ neurons would agree with the diminished inhibition to SD we observed in ARC^{AgRP} neurons after HFD access (Fig. 2). Together, this highlights the long-term impact of HFD on multiple hypothalamic nuclei and motivated feeding.

To establish whether exposure to HFD perturbs ARC^{AgRP} activity independent of sensory food detection, we longitudinally recorded population dynamics in mice either infused with calories directly into the stomach or injected with a panel of peptides/hormones before, during and after HFD challenge (Fig. 4). Infusion of non-caloric saline had no effect on ARC^{AgRP} activity over time (Figure 4a,b,d). Gastric infusion of calories (0.86 kcal of Ensure) durably reduced ARC^{AgRP} dynamics,[10,11] but we found that home cage HFD exposure severely blunted ARC^{AgRP} activity to the same caloric load during and after HFD challenge (Fig. 4c–d). This change in activity was tightly correlated to body weight after 1 week of HFD exposure but grew weaker over time (Extended Data Fig. 6a).

Given this rapid change in gut-brain communication, we reasoned that the effects of stomach-secreted peptides/hormones may no longer be as potent in modulating ARC^{AgRP} activity following HFD exposure. Indeed, while systemic ghrelin injection consistently stimulated ARC^{AgRP} neurons in mice maintained on SD, HFD-treated animals exhibited an impaired ARC^{AgRP} response to ghrelin (Fig. 4e–h); consistent with a model of HFD-induced ghrelin resistance[36,37]. However, following a 2-week HFD withdrawal, ARC^{AgRP} responses to ghrelin were not significantly different from baseline. Interestingly, while within-group deficits in ghrelin-evoked ARC^{AgRP} activity did not reach significance until 8 weeks of diet exposure, there was a significant correlation between HFD-induced weight gain and diminished ghrelin-evoked ARC^{AgRP} activity in HFD-exposed mice at 1- and 4-weeks post HFD consumption (Extended Data Fig. 6b–c). This correlation no longer existed by 8 weeks of HFD, though returned during the withdrawal period, in agreement with prior studies demonstrating body weight influence on ghrelin resistance (Extended Data Fig. 6d–e)[37].

As previously reported[10,11], we found that systemic administration of the gastrointestinal satiety signals cholecystokinin (CCK), serotonin (5-HT), or peptide YY (PYY) inhibits ARC^{AgRP} neurons over two baseline sessions while mice were maintained on SD (Figure 4j–o, Extended Data Fig. 6l–q). Mice were then maintained on SD or supplied HFD access. While all mice provided HFD rapidly gained weight, ARC^{AgRP} responses to all tested satiety signals remained intact through 4 weeks of HFD consumption (Figure 4kj–o). Further, individual changes in satiety signal responses did not correlate with HFD-induced weight gain (Extended Data Fig. 6f–k). In summary, HFD exposure rapidly remodels and impairs ARC^{AgRP} population dynamics in a manner uncoupled from sensory food detection.

HFD impairs ARC^{AgRP}-mediated SD feeding

To determine how HFD exposure affects the functionality of ARC^{AgRP}-evoked food intake, we optogenetically photoactivated ARC^{AgRP} neurons using ChR2 in mixed-sex animals (Figure 5a–c). Slice recordings revealed no overt differences in ARC$^{AgRP::ChR2}$ neurons from mice on SD versus SD + HFD diet (Figure 5b). One-hour SD consumption was measured longitudinally in fed animals near the onset of the light cycle before, during and after HFD challenge (Figure 5c). As an additional control, HFD-naïve mice were assessed over the same timeframe and showed consistent ARC^{AgRP}-induced feeding of SD across time (Figure 5d, Extended Data Fig. 7a). Conversely, HFD-exposed mice had significantly reduced stimulation-induced feeding of SD compared to both their baseline response and HFD-naïve animals at identical time points (Figure 5d, Extended Data Fig. 7a). This devaluation was independent of body weight gain over the experimental period (Extended Data Fig. 7b). Consistent with physiological hunger (Fig. 1f), SD devaluation remained after 2-week HFD withdrawal (Figure 5d, Extended Data Fig. 7a). To assess whether the observed changes in ARC^{AgRP}-evoked feeding were representative of food preference and not a generalized reduction in hunger drive, we repeated the optogenetic experiments in the HFD-exposed group in the presence of both SD and HFD (Figure 5e). Similar to natural hunger (Figure 1h), ARC^{AgRP} photoactivation promoted targeted feeding of HFD over SD, and this effect was further augmented following a 2-week HFD withdrawal period (Figure 5f, Extended Data Fig. 7c). Therefore, HFD-induced changes in ARC^{AgRP} function are severe enough to thwart SD consumption and selectively promote HFD consumption. Furthermore, these findings suggest SD devaluation may be compromised in downstream or parallel neural networks involved in food consumption.

High fat diet diminishes mesolimbic dopamine responses to SD

Mesolimbic DA is known to regulate food preference and valuation, and DA release can be altered by obesity[24,25,38,39]. To evaluate putative, direct input from ARC^{AgRP} neurons to the VTA, we employed a combination of anterograde tracing and slice connectivity experiments. Directing synaptophysin expression to ARC^{AgRP} neurons (Extended Data Fig. 8a–b) revealed dense projections to the paraventricular nucleus of the hypothalamus (PVH) but few terminals in the vicinity of tyrosine hydroxylase (TH)-positive cells of the VTA (Extended Data Fig. 8c–d). ChR2-assisted circuit mapping affirmed monosynaptic connectivity to the PVH[40] while 0 out of 45 VTA neurons recorded exhibited time-locked inhibitory post-synaptic currents (Extended Data 8e–g). To assess potential, indirect communication between ARC^{AgRP}→VTA^{Dat} neurons *in vivo*, as well as determine if devaluation of SD after HFD-exposure is encoded in the midbrain, we simultaneously transduced ARC^{Npy} and VTA^{Dat} neurons with the chemogenetic actuator hM3dq[41,42] and calcium indicator GCaMP6, respectively (Figure 6a). Due to endogenous expression of ARC$^{Dat/TH}$ neurons (Extended Data Fig. 8h), we used a Flp-dependent strategy to selectively target hM3Dq to ARC^{Npy} cells. Clozapine-N-oxide (CNO)-induced ARC^{Npy} activation rapidly drove SD intake in fed animals compared to saline vehicle injections (Extended Data Fig. 8i). Supporting our slice analyses, acute stimulation of ARC^{Npy} neurons failed to alter basal activity of VTA^{Dat} neurons (Extended Data Fig. 8j–k). Instead, we found that ARC^{Npy} activation potentiated VTA^{Dat} activity toward SD presentation (Extended Data Fig. 8l–n).

To assess whether this ARC^{Npy}-evoked response to SD was devalued following HFD exposure, we longitudinally recorded VTA^{Dat} activity in response to either SD or HFD pellets in animals before, during and after HFD challenge (Figure 6b). Baseline recordings prior to HFD challenge demonstrated increased VTA^{Dat} responses aligned to SD consumption, effects that were diminished after HFD exposure (Figure 6c–e). The response to HFD pellets remained similar throughout HFD-challenge, with a potentiation in the response following withdrawal (Figure 6f–h). Critically, after 4-week HFD challenge, the response to HFD pellets elicited a stronger VTA^{Dat} response than SD pellets (Figure 6i–k).

VTA^{Dat} stimulation is highly rewarding and leads to real-time place preference (Extended Data Fig. 9a–c)[43]. ChR2 was selectively expressed in VTA^{Dat} neurons and SD consumption was measured longitudinally before, during and after HFD exposure in fasted animals with or without light stimulation (Figure 7a–b). As we found VTA^{Dat} activity ramped up at the time of pellet retrieval (Fig. 6d–f), we transiently photoactivated VTA^{Dat} neurons as animals removed a SD pellet from the feeding device (Figure 7b). We found that VTA^{Dat} activation during pellet retrieval enhanced SD consumption in fasted, HFD-naive mice at baseline (Fig. 7c). HFD exposure strongly suppressed fasting-induced consumption of SD, even when pellet retrieval was paired with VTA^{Dat} stimulation (Figure 7c, Extended Data Fig. 9d). While SD devaluation remained after a 1-week HFD-withdrawal period, VTA^{Dat} photoactivation upon SD pellet retrieval lowered this devaluation (Fig. 7c, Extended Data Fig. 9d), suggesting this potentiation is reversible.

To pinpoint a downstream node contributing to SD devaluation, we longitudinally assessed DA release in the shell of the nucleus accumbens (AcbSh) using the DA optical sensor GRAB-DA2m in fasted mice in response to either SD or HFD pellets (Figure 8a–b)[44]. Reinforcing our ARC^{Npy}-evoked VTA^{Dat} recordings above, DA release during SD pellet approach/retrieval was bolstered in fasted versus fed animals (Extended Data Fig. 10a–c). Following 1 week of HFD access, SD approach/retrieval resulted in reduced DA release compared to Baseline (Fig. 8c–e). Critically, DA release to SD remained consistent over time in HFD-naïve mice (Extended Data Fig. 10d–f). This DA-evoked devaluation of SD persisted throughout HFD exposure and started to approach Baseline levels after HFD-withdrawal (Fig. 8c–e). DA release in response to HFD pellets remained comparable across time in the same animals that exhibited SD devaluation (Fig. 8f–h). Supporting the notion that DA shapes the value of food, HFD-exposed animals demonstrated a larger response to HFD versus SD pellet approach/retrieval at 1 week of HFD challenge (Fig. 8i–k). Collectively, these data demonstrate a robust plasticity in multiple neural circuits that contributes to food devaluation helping explain the challenges of dieting in an obesogenic environment.

Discussion

Despite an ever-expanding number of new diets, many people who are successful in adopting healthier lifestyles often return to old eating habits. Here, we reveal fatty food-altered responsivity and functional drive of ARC^{AgRP} and VTA^{Dat} neurons toward SD, corresponding with devaluation that persists despite HFD removal, a condition analogous to a strict diet. These chronic and recalcitrant circuit adaptations illuminate the underlying

difficulty in dieting as hypothalamic and mesolimbic neural circuits, encoding negative and positive affective states, respectively, now produce a sustained multifaceted tuning toward calorically dense food.

Homeostatic food-seeking is generated by ARC^{AgRP} neurons through an interoceptive negative valence signal that is relieved by sensory detection of food and subsequent consumption[12]. We observed that HFD challenge diminishes ARC^{AgRP} neurons responses to SD both before and after consumption, thus preventing alleviation of the negative valence signal and promoting continued seeking of an alternative food source. Similarly, ARC^{AgRP} neuron responses to peripheral nutritional status were impaired even when an equal caloric load was directly infused into the stomach, suggesting that a history of HFD consumption may set a steeper caloric requirement to fully alleviate ARC^{AgRP} activity. These findings underlie a developing disconnect between functional ARC^{AgRP} responses to signals of hunger and satiety and actual caloric content. Upstream neural adaptations may play a role as well, as demonstrated by HFD-induced alterations in DMH^{LepR} responses to food and presynaptic release. Importantly, re-exposure to HFD after withdrawal induced robust feeding and stronger inhibition of ARC^{AgRP} neurons under conditions of satiety, providing an avenue for ARC^{AgRP} neurons to promote binge-like consumption during dietary relapse even in the absence of hunger.

A caveat of fiber photometry recordings is the inability to resolve individual cellular activity. Although calcium recordings of ARC^{AgRP} activity demonstrate homogenous responses to food[12], *in vivo* electrical recordings[8] and projection-specific activation studies[45] suggest potential heterogeneity that cannot be captured with this technique. Nonetheless, our spectrum-based approach is optimized for longitudinal recordings to control for changes in GCaMP6 expression over time and HFD-induced inflammation[1]. This approach enabled the discovery that HFD exposure significantly diminishes basal ARC^{AgRP} activity. Interestingly, acute alcohol and non-nutritive drugs lead to ARC^{AgRP} inhibition[17] perhaps implicating a common mechanism through which prolonged exposure to drugs of abuse, including HFD, can negatively shift ARC^{AgRP} basal activity. Localizing the sources contributing to this depression will be subject to future studies.

In addition to homeostatic eating, we observed changes in hedonic drive as reflected by changes in mesolimbic dopamine signaling. Although we observed no evidence of direct communication between $ARC^{AgRP} \rightarrow VTA^{Dat}$ neurons, we report that both physiological and artificial hunger potentiate DA signaling to food[17]. The HFD-induced devaluation of SD observed in the DA system described here aligns with prior work exhibiting changes in basal midbrain DA activity, projections, and release following palatable diet exposure[19,25,46,47]. Going forward, it will be important to determine whether DA accumbal signaling loses reinforcement properties independent of food discovery after HFD exposure. Interestingly, the magnitude of the DA response to HFD was similar to the response to SD prior to HFD exposure, possibly suggesting that HFD had displaced the value of SD for fasting-induced motivated feeding. Of note, activity of dorsal and ventral striatal circuits can reflect nutritional and hedonic value of food, respectively[39,47]. While imaging studies have not been performed in adult human patients naïve to fatty food, our findings are similar to enhanced striatal DA activity observed in obese subjects presented with images of calorically dense

food[20–22]. Studies in human patients further showed diminished striatal function during food consumption and weight gain and were tied to deficits in D2R expression[48,49]. Critically, our work relies on a D2R-mimicking DA sensor and allows us to detect DA release independent of endogenous D2 availability. Together, our observed functional alterations in homeostatic and hedonic circuits provide a mechanistic blueprint for the obstinate challenges associated with dieting in an environment rich with energy-rich foods.

Methods

Animals

C57BL/6J mice, *Agrp*$^{tm1(cre)Lowl}$/J (Stock No: 012899), B6.SJL-*Slc6a3*$^{tm1.1(cre)Bkmn}$/J (Stock No: 006660), B6;129S4-*Mc4r*^{tm1Lowl}/J (Stock No: 006414), B6.Cg-*Lep*^{ob}/J (Stock No: 000632) and *LepRb*$^{(cre)}$ mice were used. Mice were housed with a 12 h light/dark cycle with *ad libitum* access to water and standard chow (Envigo 7017 NIH-31, 14% kCal from fat) unless otherwise stated. In some cases,, *Agrp*$^{tm1(cre)Lowl}$ were crossed with B6.Cg-*Gt(ROSA)26Sor*$^{tm9(CAG-tdTomato)Hze}$/J (Stock No: 007909)[50] to generate AgRP-Ai9 reporter mice for use with spectrometer-based *in vivo* fiber photometry recordings. *LepRb*$^{(cre)}$ mice were crossed with *B6.FVB-Tg(Npy-hrGFP)1Lowl/J* (Stock No: 006417) and *Agrp*$^{tm1(cre)Lowl}$ were crossed with *B6; 129S-Gt(ROSA)26Sor*$^{tm32(CAG-COP4*H134R/EYFP)Hze}$*/J* (Stock No: 012569) to generate mice for ephys studies. B6.Cg-*Npy*$^{tm1.1(flpo)Hze}$/J (Stock No:030211) mice were crossed with B6.SJL-*Slc6a3*$^{tm1.1(cre)Bkmn}$/J (Stock No: 006660) for combinatorial chemogenetic and photometric recordings. All animal protocols and procedures were approved by the US National Institute of Environmental Health Sciences Animal Care and Use Committee or the National Institutes of Health Animal Care and Use Committee. Mice were group-housed prior to the start of experiments and were transferred to single housing following stereotaxic surgery or during home cage feeding measures. After baseline recordings where mice had *ad libitum* access to water and standard chow, a select group was put on *ad libitum* access to water, standard chow, and high-fat diet (Research Diets D12492, 60% kCal from fat) for the duration of the experimental period. During the withdrawal period all mice had *ad libitum* access to water and standard chow All experiments were carried out in adult (>8 weeks) male and female mice with the exception of optogenetic stimulation of VTA^{DA} neurons, which only used males.

Viral Vectors

AAV1-hsyn-FLEX-GCaMP6s (Addgene v100845) was used for spectrometer-based fiber photometry recordings of AgRP-positive ARC neurons and recordings of DAT-positive VTA neurons. For DA sensor recordings, AAV9-hsyn-GRAB-DA2m (Vigene) was mixed with AAV9-hsyn-tdTomato (NIEHS Viral Vector Core) at a ratio of 5:1 prior to injection. AAVrh10-CAGGS-FLEX-ChR2-tdTomato-WPRE-SV40 (Addgene 18917) was used with optogenetic stimulation experiments to stimulate AgRP-positive neurons in the ARC and LepR-positive neural projections to the ARC. AAV5-hSyn-hChR2EYFP(H134R) (Addgene 26973) was used with optogenetic stimulation experiments to stimulate DAT-positive neurons in the VTA. AAV1-CAG-FLEX-X-jG-GCaMP7s-WPRE (Addgene 104495) was used with *in-vivo* fiber photometry experiments to longitudinally record from AgRP-positive

neurons in the ARC during gastric infusion. AAV5/2-hSyn-dFRT-hM3dq-mCherry (VVF University of Zurich v189–5) was used for chemogenetic activation experiments of Npy/AgRP positive neurons in ARC. All viruses had a titer of $>10^{12}$ viral particles per ml.

Viral injections

Stereotaxic injections were performed as previously described[51]. Mice were anesthetized with isoflurane and placed into a stereotaxic apparatus (Kopf Instruments or Stoelting Instruments). After sterilization of the incision site with ethanol and Betadine, the skull was exposed via a small incision. Small burr holes were drilled above the microinjection target sites. A 2μl Neuros Hamilton Syringe with a 30-gauge needle was used to microinject virus into the target sites at a rate of 100 nl/min using a syringe pump (World Precision Instruments). The needle was slowly withdrawn 5 minutes following the completion of the injection to reduce backflow of the virus. Target coordinates relative to Bregma (in mm) and viral volumes injected were: ARC (AP: −1.50 to −1.55, ML: ± 0.30, DV: −5.85, 700 nl per side). AcbSh (AP: 1.00, ML: ±1.70 to 2.00, DV: −4.40 to −4.60, 400 nl per side). Following surgery, the incision was closed using surgical sutures. In some cases, viral injections were performed using a pulled glass pipette, as previously described[6]. In these cases, the following coordinates were used. ARC coordinates: AP −1.45mm, ML +/− 0.25mm, DV −5.75mm and −5.65mm (300 nl per side). VTA coordinates: AP −3.05mm, ML +/− 0.35mm, DV −4.45mm and −4.25mm (150 nl unilaterally). DMH coordinates: AP −1.80mm, ML +/− 0.30mm, DV −5.2mm.

Intragastric Catheter Implantation

Agrp-IRES-Cre mice that were already implanted with an optical fiber were anesthetized with isoflurane. Abdominal midline incisions were made through the skin and muscle layers separately. 8mm gastric catheters made of Micro-Renathane tubing with epoxy balls on each end (Braintree Scientific, MRE-033, 0.033 × 0.014 in) were implanted in the fundus and secured with surgical mesh (Bard, 0112660) glued with liquid adhesive (Devcon Clear Epoxy Adhesive, 92926). This procedure was adopted from previous work[11]. The abdominal layer was stitched with Coated Vicryl Violet Braided Sutures 5–0 (Ethicon, J385H) while the skin layer was closed with 9mm wound clips using a MikRon 9mm autoclip applier (Braintree Scientific 205016, 205000). Mice were treated post-operatively with buprenorphine slow-release analgesia (1.2mg/kg subcutaneously). Mice for gastric infusions were allowed two weeks from time of catheter implantation to recover, with a periodic flush of deionized water to keep the catheter from clogging with food particles.

Drugs

Ghrelin (Tocris, 1465), CCK octapeptide (Bachem, CAT: 4033010), PYY 3–36 (R&D Systems, Cat#1618), and 5-hydroxytryptamine hydrochloride (5-HT; Sigma-Aldrich, Cat#H9523), were dissolved in saline at stock concentrations and stored at −80°C until use. On the day of testing, the stock was thawed, diluted with saline, and delivered at a volume of 10 ml/kg at the following doses: ghrelin (1 mg/kg), CCK (10 μg/kg), 5-HT (2 mg/kg), and PYY (0.1 mg/kg).

Spectrometer-based fiber photometry system

For *in vivo* fiber photometry recordings of ARC^{AgRP} neuron responses to home cage food presentation, ghrelin, gastrointestinal satiety signals, and accumbal DA release with a fluorescent DA sensor, we used a spectrally resolved fiber photometry system as described previously[51]. Briefly, a laser beam from a 488 nm 60 mW continuous wave (CW) laser (OBIS 488LS-60, Coherent, Inc.) was aligned into a fluorescence cube and reflected using a dichroic mirror (ZT488/561rpc), Chroma Technology Corp) into the core of a multimode patch cable (M72L05, Thor Labs). This patch cable was connected to an optical joint (FRJ_1×1, Doric Lenses) followed by a second patch cable that ended with an FC ceramic ferrule (200μm core diameter, 0.39NA; M83L01, Thor Labs) This patch cable could be connected to an optical probe implanted with the mouse via coupling with a ceramic split sleeve (SM-CS125S, Precision Fiber Products Inc.). Emission was collected by the optical fiber tip, then passed through the same patch cables before passing through the dichroic of the filter cube. Here, the emitted light was routed into an AR-coated multi-mode patch cable connected to the entrance port of a spectrometer (QE Pro-FL, Ocean Optics, Inc.). Spectral data were acquired by OceanView software (Ocean Optics, Inc.). In rare cases, a 561 nm 60 mW CW laser (OBIS 561LS-60, Coherent, Inc.) was used simultaneously to increase red fluorescence emission in tdTomato. Light intensity outputs as measured at the end of the final patch cable tip were adjusted to be 50–70 μW for 488 nm excitation and 40 μW for 561 nm excitation when used.

Optical fiber implantation

For spectrometer-based fiber photometry recordings, optical fiber implants were constructed by threading an optical fiber (200 μm, 0.39 NA; FT200EMT, Thor Labs) through a ceramic ferrule with a 1.25 mm OD (MM-CON2007–2300, Precision Fiber Products) and secured with heat-cured epoxy (Epoxy 353ND, Precision Fiber Products), then polished and cleaved to length. At least 3 weeks following viral injection surgery, mice underwent a second stereotaxic surgery to receive a unilateral implantation of the optical fiber. The optical fiber was connected to a patch cable (200 μm, 0.39NA, Thor Labs) using a ceramic split sleeve (SM-CS125S, Precision Fiber Products Inc.), which was connected to the spectrometer-based photometry system with blue (488 nm) illumination (50–70 μW). This allowed for real-time visualization of fluorescent emission signal of GCaMP and tdTomato, or DA2m and tdTomato, during probe implantation. After the mouse was anesthetized on the stereotax and the skull exposed, a burr hole was drilled above the target site (ARC or AcbSh). The optical fiber was lowered to the ARC (GCaMP-based experiments) or lateral AcbSh (DA2m-based experiments) slowly until a maximum fluorescent signal was obtained. If no fluorescent emission signal was observed, the probe was slowly retracted, cleaned with sterile saline and lens paper, then lowered into corresponding target structure of the opposite hemisphere. Once positioned, the optical fiber was secured to the skull using Metabond (Parkell). Mice were then placed into single housing for the remainder of experiments. Mice recovered for at least 1 week before the start of recording sessions. For fiber implantation in the ARC for photostimulation experiments: AP −1.45mm, ML +/− 0.25mm, DV −5.40mm. For fiber implantation in the VTA for photostimulation experiments: AP −3.05mm, ML +/− 0.35mm, DV −4.05mm. For fiber implantation in the ARC for *in-vivo* photometry recordings with gastric infusions: AP −1.45mm, ML +/− 0.22mm, DV −5.60mm.

AgRP home cage photometry

AgRP-Ai9 mice expressing GCaMP6s in ARC^{AgRP} neurons were handled by the experimenter at least 1 week prior to the start of recordings. Body weights and home cage food intake were measured at least weekly. Photometry recordings were conducted during the light cycle, and mice were transferred to a new home cage the night before testing. During photometry recordings, nestlets were removed from the home cage to aid in visualization of the bedding and were returned to the home cage upon completion of the recording trial. A patch cable (detailed above) was connected to the optical fiber implant, and the home cage was placed in a sound attenuating box with illumination from the Med Associates house light. Fluorescence spectra that included GCaMP and tdTomato were acquired using a 19 ms integration time and were triggered at 25 Hz TTL pulses sent from a digital output module (DIG-726TTL, Med-associates, Inc.) A digital video camera (Grasshopper3 GS3-U3–23S6M-C, FLIR, Integrated Imaging Solutions, Inc.) captured the entire home cage during recording and was triggered frame by frame by the same TTL pulses. This allowed us to match each video frame with the corresponding fluorescence signal.

ARC^{AgRP} photometry responses were tested repeatedly across 3 types of recording sessions: Ghrelin, Fed, and Fasted. In all conditions, mice were recorded for 15 minutes prior to either a ghrelin injection or the addition of food to the cage. For Ghrelin recordings, mice received a 1 mg/kg intraperitoneal injection of ghrelin and were returned to the home cage for 5 minutes. During Fed recordings, following the 15-minute period, a pre-weighed chow pellet was added to the corner of the home cage. Recording continued for 5 minutes, after which a second pre-weighed chow pellet (Chow Group for all sessions, B1 and B2 time points for HFD group), or HFD (HFD group, 1 week, 4 weeks, 8 weeks, and Withdrawal time points) was added to the cage. The weight of the first pellet was determined at this time and it was returned to the home cage. The recording continued for 5 minutes after the addition of the second pellet. Fasted recordings were identical to Fed recordings with the exception that mice were food deprived beginning ~18 hours before the recording session.

AgRP responses to intraperitoneal administration of the gastrointestinal satiety signals CCK (10 μg/kg), 5-HT (2 mg/kg), and PYY (0.1 mg/kg) were tested in a separate cohort of mice. Mice were fasted ~18 hours prior to the recording sessions. To reduce the number of required overnight fasts, we tested each mouse's response to all 3 compounds on the same day. Recordings were separated by at least one hour per drug per mouse, and always in the order of CCK, 5-HT, then PYY, as only PYY had long-lasting inhibition of AgRP neurons. Following PYY testing, mice were immediately returned to ad libitum access to their home cage diets until the next testing session, which was at least one week later.

AgRP home cage photometry data analysis

Raw emission spectra data were passed through a spectral linear unmixing algorithm written in R that has been detailed previously[51]. To correct for motion artifacts, unmixed coefficient values for GCaMP were normalized to the unmixed coefficients for tdTomato to generate a GCaMP/tdTomato ratio values that were treated as F. %dF/F were calculated using the formula: $(100 * (F-F_0)/F_0)$ where F is the fluorescent ratio value of a given frame and F_0 was

defined as the mean F value during the 5 minutes prior to when a hand entered the video frame to pick up the mouse for a drug injection or to add the first food pellet. Quantified responses to ghrelin and Pellet 1 were measured as the mean %dF/F value during the last 2 minutes during the 5 minutes following the injection or pellet addition (Minutes 3–5). %dF/F changes during Pellet 2 were calculated similarly and reported as the difference from the Pellet 1 response. For photometry measurements aligned to the first bite of food, the calculated %dF/F values were aligned to the first frame of a visible feeding bout occurring within the first 5 minutes of pellet addition, and the average %dF/F one second prior to the bite was calculated. Sessions where mice did not consume the SD pellet during these 5 minutes were excluded from bite-alignment analyses, which only occurred in mice from sessions following HFD exposure. For satiety signal experiments (CCK, 5-HT, and PYY), the mean %dF/F value during the first 10 minutes post-injection (mins 0–10), and next 10 minutes post injection (mins 10–20) were averaged. Correlations between photometry measurements and body weight changes across weeks were calculated by normalizing the photometry response on a given week to the individual mouse's average across the baseline B1 and B2 sessions, while weight was normalized to the body weight of each mouse on the day it first received access to HFD, or the matching timepoint for SD-only control mice.

In animals that were placed under gastric infusion experiments, no spectral unmixing algorithm was applied due to lack of tdTomato, but %dF/F were calculated using the formula: $(100 * (F-F_0)/F_0)$ where F is the fluorescent ratio value of a given frame and F_0 was defined as the mean F value during the 5 minutes prior the infusion. Quantified responses to infusion were measured as the mean %dF/F value during the last 2 minutes during the 10 minutes following start of infusion (Minutes 5–15) and during the last 2 minutes during the 10 minutes following pellet addition (Minutes 15–25).

VTA DA home cage photometry

Npy-FlpO;DAT-cre mice expressing hM3dq in the ARC and GCaMP6s in the VTA were handled by the experimenter for one week prior to experiments and mice were housed with a small white ramekin always present in their home cages. Experiments were conducted in the home cage at 09:00–11:00, near the beginning of the light cycle when food intake is normally low. Basal activity recordings were completed over two days with counterbalanced saline and clozapine N-oxide (CNO) conditions on any given day. Mice were tethered to a patch cable and basal activity was recorded for 5 minutes (baseline) before injection and for 30 minutes post-injection. For food response recordings, the cage was changed to remove all food, mice were then injected 30 minutes before recording, and their small ramekin was placed in the corner of the home cage. Food response recordings were completed over two days: one day being the injection of CNO with SD pellet drops, and the other day being the injection of CNO with HFD pellet drops. During the food response recordings, the experimenter dropped small SD or HFD food pellets (0.05g each) into the ramekin. Food was not dropped if the mouse was sitting inside the ramekin.

VTA DA home cage photometry analysis

For basal activity recordings, the overall traces were fit to and subtracted by a regression line to minimize photobleaching. For food response recordings, video frames were analyzed to

determine the time at which the mouse retrieved the pellet prior to consumption, which was defined as when the mouse had taken the pellet and assumed a stereotypical hunched posture during feeding. This was defined as time 0 for each retrieval event. The mean and maximum Z-score were used for the traces, normalized to a baseline period of 60 seconds before each event. The normalized mean and maximum Z-score for 3 seconds after retrieval (when observed activity is highest) were used for quantification. For each mouse, we averaged the results of the first 5 pellet retrievals, though the mice could retrieve up to 10 pellets per session. This was done to minimize satiety-related decreases in retrieval fluorescent Z Scores during later pellet retrievals.

Screening protocol for chemogenetic activation experiments

Npy-IRES2-FlpO;DAT-cre mice expressing hM3dq in the ARC and GCaMP6s in the VTA were handled by the experimenter for one week prior to experiments. Screening for all Npy-IRES2-FlpO;DAT-cre mice was conducted in the home cage at 09:00–11:00, near the beginning of the light cycle when food intake is normally low, and was completed over two days. On any given day, injections were counterbalanced, with half of the mice receiving a saline injection and the other half receiving a clozapine N-oxide (CNO) injection. After 30 minutes post-injection, food was given in the home cage and measured after 30 minutes of access.

DA sensor photometry testing

Recordings were carried out in an open-top mouse operant chamber with a white plastic floor (21.6 × 17.8 × 12.7 cm, Med-Associates, Inc.) housed in a sound attenuating box. A small petri dish was placed in a corner beneath a chute connected to a rubber tube that ran outside of the sound attenuating box. This chute allowed for small food pellets (20–25mg) to be dropped into the petri dish without an experimenter reaching into the box during recordings. Mice were habituated to the box with food in the dish for at least 10 minutes prior to the first testing day. Photometry recording settings and equipment were identical to those used for ARC^{AgRP} GCaMP recordings. In each recording session, mice were connected to the patch cable and placed in the testing arena for 15 minutes without food available in the dish. Video recording of the session began during the last 5 minutes of this period. After this time, the experimenter supplied one food pellet (chow or HFD depending on the session). Retrieval of the food was visualized live and the experimenter waited at least 60 seconds following retrieval before the addition of another pellet. Pellets were not added if the mouse was sitting in the petri dish. Each session lasted for up to 50 minutes (including the 15-minute period without food) or 10 pellet retrievals. A maximum of 4 potential recording conditions were tested in a given week: Sated-Chow, Sated- HFD, Fasted-Chow, Fasted-HFD. Only one type of food was ever tested within a test session. Floors and walls of the test chamber were cleaned with 70% ethanol between mice.

DA sensor photometry analysis

Raw DA2m and tdTomato signals were unmixed using the algorithm described above. Video frames were analyzed to determine the frame in which the mouse retrieved the pellet and prior to consumption, which was defined as when the mouse had taken the pellet and assumed a stereotypical hunched posture during feeding. This was defined as time 0 for each

retrieval event. Using custom R software, 90-second windows around each event were individually analyzed and split into 4 behavioral events: Baseline (−45 to −30s), Approach/Retrieval (−2 to 0s), Consumption (1 to 6s), and Post-Consumption (30 to 45s). For each retrieval event, the mean and standard deviation of the GCaMP/tdTomato ratio during the baseline event was calculated and used to convert each 90-second window into fluorescent Z-score values. The mean Z-score within the behavioral windows were used for quantification. For each mouse, we averaged the results of the first 5 pellet retrievals, though the mice could retrieve up to 10 pellets per session. This was done to minimize satiety-related decreases in Approach/Retrieval fluorescent Z Scores during later pellet retrievals during Fasted test sessions.

In-vivo Photostimulation

Fiber optic cables (200mm diameter, Doric Lenses) coupled to lasers were attached to the fiber cannula of the mice via zirconia sleeves (Doric Lenses). Light was delivered to the brain through an optical fiber (200um diameter core; CFMLC22U-20, Thor Labs). Light power exiting the fiber tip was 10mW for both the ARC and VTA.

For photostimulation of AgRP-positive neurons in the ARC, pulse trains (20HZ; 2 sec on, 2 sec off; 473nm from Laserglow laser technologies) were programmed using a waveform generator (PCGU100; Valleman Instruments) for continuous photostimulation during all tasks. All AgRP photostimulation experiments were conducted at 08:00–11:00 hours, near the beginning of the light cycle when food intake is low.

For photostimulation of DAT-positive neurons in the VTA during real-time place preference, pulse trains (20HZ, 250ms on, 250ms off; 473nm from Laserglow laser technologies) were custom programmed with Arduino electronics and continued for as long as the mouse remained on the side of the chamber associated with photostimulation. For photostimulation of the VTA during the fast-refeed task, pulse trains (20HZ, 250ms on, 250ms off; 473nm from Laserglow laser technologies) were custom programmed with Arduino electronics and continued for 5 seconds after each pellet retrieval. All *DAT-Cre* mice were fasted overnight for 18 hours and photostimulation experiments were conducted at 09:00–12:00 the next morning.

Screening Protocols for Photostimulation

Screening for all *Agrp-IRES-Cre* mice was conducted in the homecage at 08:00–11:00, near the beginning of the light cycle when food intake is normally low. After tethering and a 20-minute acclimatization period, mice were given *ad-libitum* access to standard chow for a 20-minute baseline, followed by *ad-libitum* access to standard chow for a 20-minute photostimulation period (as described). Only mice that have eaten >0.30g of standard chow during the photostimulation period were selected for the experiments.

Real-time place preference (RTPP) was conducted to screen all *Dat-IRES-Cre* mice and was conducted at 09:00–12:00. The RTPP chamber was built of white plexiglass walls/floor (50×26×30cm) with a middle partition providing equal separation of the two sides. Mice could move freely between the two sides. One side of the chamber was paired with photostimulation (as described) while the other side of the chamber was not. Only mice that

have spent >55% of their time on the photostimulation side were included in the study. Movement tracking was completed using Ethovision XT 14 software (Noldus Inc).

Food Intake and Weight Change Measurements

Male and female C57BL/6J mice had *ad libitum* access to water and standard chow for 10 days before they were either kept on *ad libitum* access to water and standard chow, or put on *ad libitum* access to water, standard chow, and high-fat diet (Research Diets D12492, 60% kCal from fat) for 8 weeks. Mice were then all kept/put on *ad libitum* access to water and standard chow only for 2 weeks. During this time, food intake and weights of mice were measured daily. Lean and fat mass measurements were taken weekly using quantitative magnetic resonance (QMR) spectroscopy (EchoMRI 3-in-1). During fast-refeed experiments, mice were fasted overnight for 18 hours and given access to either standard chow or both standard chow and high-fat diet for one hour between 09:00–11:00.

Timed Photostimulation During Fast-Refeed

All trials were conducted in a Phenotyper (Noldus Inc) used as a homecage and recorded/managed through Ethovision XT 14 software (Noldus Inc). Each Phenotyper homecage contained a Feeding Experimentation Device (F.E.D.), an automated food dispenser[52]. F.E.D.s dispensed 20mg chow pellets (TestDiet) and monitored retrieval of each pellet by the mice. Mice were habituated with the F.E.D. for three days before testing began. All animals were fasted for 18 hours, then given access to the F.E.D. for one hour with or without stimulation. Upon retrieval of one 20mg pellet, photostimulation at the described light pulse train lasts for 5 seconds, followed by an intertrial interval of 15 seconds during which the mouse cannot retrieve another pellet.

Electrophysiology

To prepare brain slices for electrophysiological recordings, brains were removed from anesthetized mice (4–8 weeks old) and immediately submerged in ice-cold, carbogen-saturated (95% O_2, 5% CO_2) sucrose solution (in mM): 87 NaCl, 75 sucrose, 25 glucose, 25 $NaHCO_3$, 7.5 $MgCl_2$, 2.5 KCl, 1.25 NaH_2PO_4, and 0.5 $CaCl_2$. Then, 300-μM thick coronal sections of the arcuate nucleus were cut with a Leica VT1000S Vibratome and incubated at 32 °C in oxygenated aCSF for 60 min (in mM): 125 NaCl, 25 $NaHCO_3$, 11 glucose, 2.5 KCl, 1.25 NaH_2PO_4, 1 $MgCl_2$, and 1 $CaCl_2$ (~308 mOsm/L). Slices were maintained and recorded at room temperature (20–24 °C). For voltage-clamp recordings, intracellular solution contained the following (in mM): 70 K-gluconate, 80 KCl, 10 HEPES, 1 EGTA, 4 Na_2-ATP, and 0.4 Na_2-GTP, pH 7.35 and 290 mOsm. For current-clamp recordings, intracellular solution contained the following (in mM): 130 K-gluconate, 10 KCl, 0.3 $CaCl_2$, 1 $MgCl_2$, 10 HEPES, 1 EGTA, 10 Na-Phosphocreatinine, 3 Mg-ATP, and 0.3 Na_2-GTP, pH 7.35 and 290 mOsm.

Light-evoked IPSCs were isolated with kynurenic acid (3mM) and recorded in the whole-cell voltage-clamp mode, with membrane potential clamped at −70 mV. All recordings were made using a Multiclamp 700B amplifier, and data was filtered at 2 kHz and digitized at 10 kHz. To photostimulate channelrhodopsin2-positive fibers, a high power white LED light source (Prizmatix) in combination with blue light filter was used. The blue light was focused

onto the back aperture of the microscope objective, producing a wide-field exposure. The light output was controlled by via TTL output through pClamp 10.2 software (AXON Instruments). Photostimulation-evoked IPSC paired-pulse ratio protocol comprised 2 blue light laser pulses (pulse duration, 2 ms) administered 200ms apart, repeating for an average of 20 sweeps per cell. Paired-pulse ratio was calculated by peak amplitude (pulse2/pulse1). Light-evoked action potentials were recorded in the whole-cell current-clamp mode. Photostimulation of 10ms pulse width was triggered at 10 Hz and 20Hz.

Intragastric Infusions

All trials were conducted in the homecage between 09:00–12:00 after an overnight fast of 18 hours. Implanted gastric catheters were connected to Micro-Renathane tubing (3ft, Braintree Scientific, MRE-033, 0.033 × 0.014 in) and a 5mL luer lock syringe placed into a pump (New Era Pump Systems, NE-1000). After a baseline period of 5 minutes, 1 mL infusions of either 0.9% saline or 0.86 kCal Ensure were completed over 10 minutes at a rate of 0.1 mL/min.

Immunohistochemistry

Mice were transcardially perfused with ice cold 30 mL of PBS, followed by 30 mL of 4% PFA. Subsequently, the brains were extracted and left in 4% PFA overnight. Following overnight post-fixation, the brains were transferred to PBS from which they were coronally sectioned at 45 μm using a Leica VT1200S vibratome. The brain slices were rinsed 3 times with PBS before undergoing blocking and permeabilization with 10% goat serum in 0.4% Triton-X for one hour. They were then left to incubate overnight at 4°C with primary antibodies diluted in PBS (1:1000). The primary antibodies used were chicken anti-GFP (ab13970, Abcam) for detecting GCaMP6s and rabbit anti-RFP (ab62341, Abcam) for detecting tdTomato. For the nucleus accumbens samples, anti-RFP antibodies were not used due to there being profuse tdTomato expression following viral injection. On the following day the slices were rinsed 3 times with PBS and incubated in secondary antibodies diluted in PBS (1:500) for one hour. The secondary antibodies used were Alexa Fluor 488 conjugated goat anti-chicken (A11039, Invitrogen) and Alexa Fluor 568 conjugated goat anti-rabbit (A11011, Invitrogen). After 3 washes with PBS, the brain slices were mounted on slides and coverslipped with VECTASHIELD Hardset Antifade Mounting Medium with DAPI. Images were taken using a Zeiss automated inverted epifluorescent microscope (10x, NA = 0.3) and a Zeiss LSM 710 inverted confocal microscope (20x, NA = 0.8). Zeiss's Zen software was used to acquire and process the images. A mouse anti-TH antibody (1:1000; Product ID : 22941, Immunostar) followed by labeling with an Alexa Fluor 488 conjugated goat anti-mouse (AB150113, Abcam) was used for imaging TH expression.

Statistics and reproducibility

GraphPad Prism 8 was used for statistical analysis and generation of graphs. SPSS was used for a 3-Way ANOVA comparison for assessing baseline differences in ARC^{AgRP} activity between SD/HFD groups across recording weeks between the fed and fasted states. For discrete comparisons between two groups, two-tailed t tests were used. For comparisons across groups or between groups over time, repeated measures one-way or two-way ANOVAs were used, respectively, with corresponding post hoc tests adjusted for multiple

comparisons. Normality and equal variances were assumed. Mice were randomly assigned to groups but were matched for age, sex, and body weights. Experimenters were not blinded to conditions during testing and analysis due to the necessity to only test HFD-exposed mice with HFD access, as well as the visibly clear differences in body weights after chronic HFD. Power analyses were not used to determine sample sizes, however group sizes were chosen to match similar studies[9–11].

Extended Data

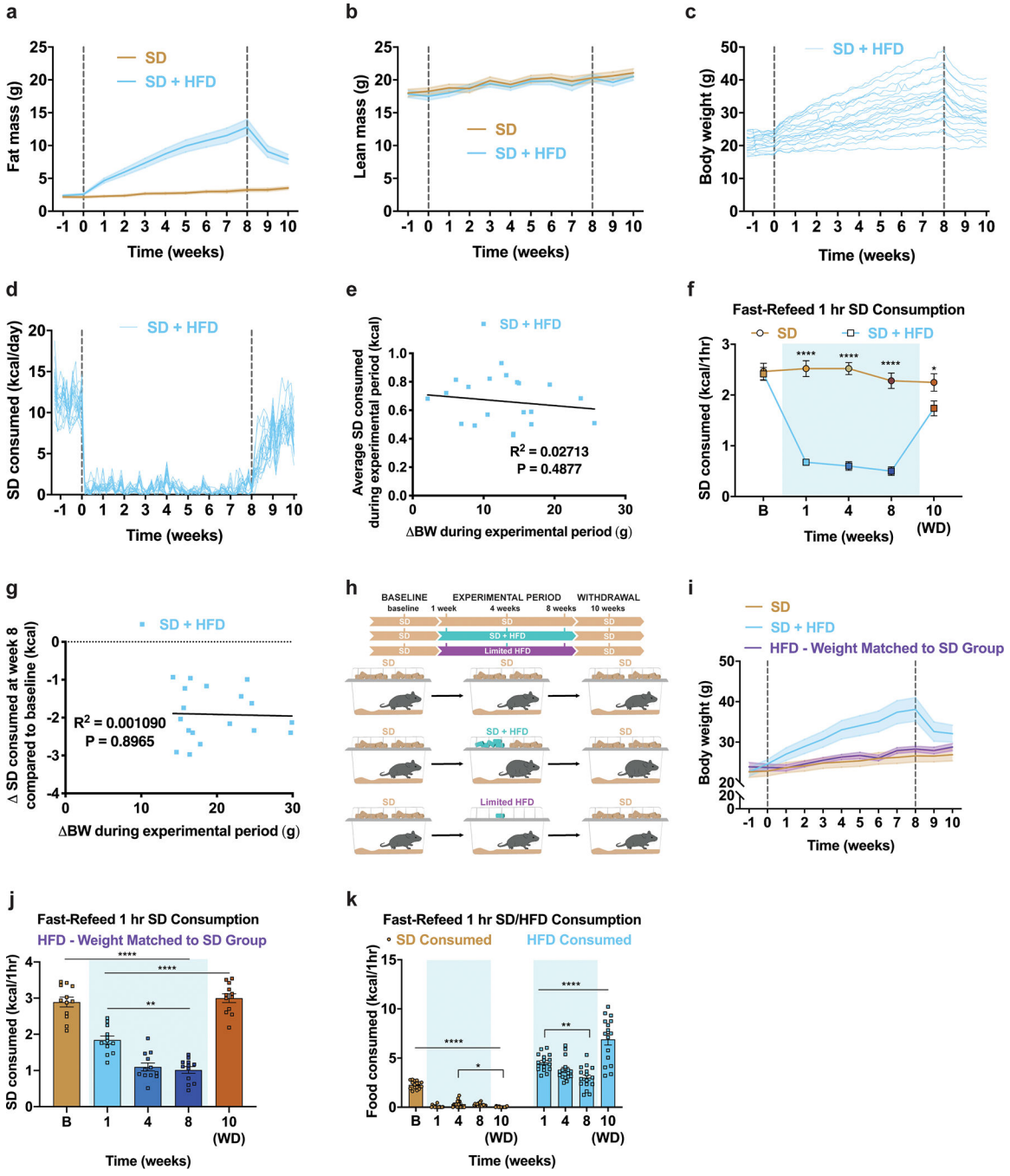

Extended Data Fig. 1: HFD-exposure promotes fat mass accrual, reduction of homecage SD intake and devaluation of SD in physiologically hungry mice independent of weight gain.

Weekly **a,** fat mass (n=20, males and females, RM two-way ANOVA, Week x Group: $F(11, 418) = 50.17$, $P<0.0001$, Sidak's multiple comparisons test) and **b,** lean mass throughout diet exposure (n=20, males and females, RM two-way ANOVA, Week x Group: $F(11, 418) = 0.8075$, $P=0.6326$). Daily **c,** body weights and **d,** SD intake throughout the duration of the experiment of individual animals exposed to HFD. **e,** No correlation between the average

amount of SD intake during the HFD-exposure period and body weight changes after 8 weeks of SD and HFD access (n=20, males and females, Linear regression, R^2= 0.02713, P=0.4877). **f,** Between-subject comparison of 1 hr SD fast-refeed consumption across test sessions (n=16 SD group, n=18 SD + HFD group, males and females, RM two-way ANOVA, Time x Group: F (4, 128) = 28.99, P<0.0001, Bonferroni's multiple comparisons test). **g,** No correlation between SD devaluation at Week 8 relative to Baseline and body weight changes after 8 weeks of access to SD and HFD (n=18, males and females, Linear regression, $R^{2=}$0.001090, P=0.8965). **h,** Experimental timeline, group schematic for home cage measurements and **i,** and daily body weights throughout the duration of the experiment (n=12 per group, males and females). **j,** Within-subject comparison of 1 hr SD fast-refeed consumption across testing sessions (n=12 limited HFD weight-matched to SD group, males and females, RM one-way ANOVA, Time: F (2.431, 26.74) = 66.81, P<0.0001, Tukey's multiple comparisons). **k,** Within-subject, within-diet comparisons of 1 hr SD and HFD fast-refeed consumption across testing sessions (n=18, males and females, RM one-way ANOVAs, Tukey's multiple comparisons). Dotted lines in **a, b, c, d** and **i** delineate window of HFD availability. All error bars and shaded areas in **a, b** and **i** represent mean ± s.e.m. Shaded blue area in **f**, **j**, and **k** represent HFD homecage availability. *$P < 0.05$, **$P < 0.01$, ****$P < 0.0001$.

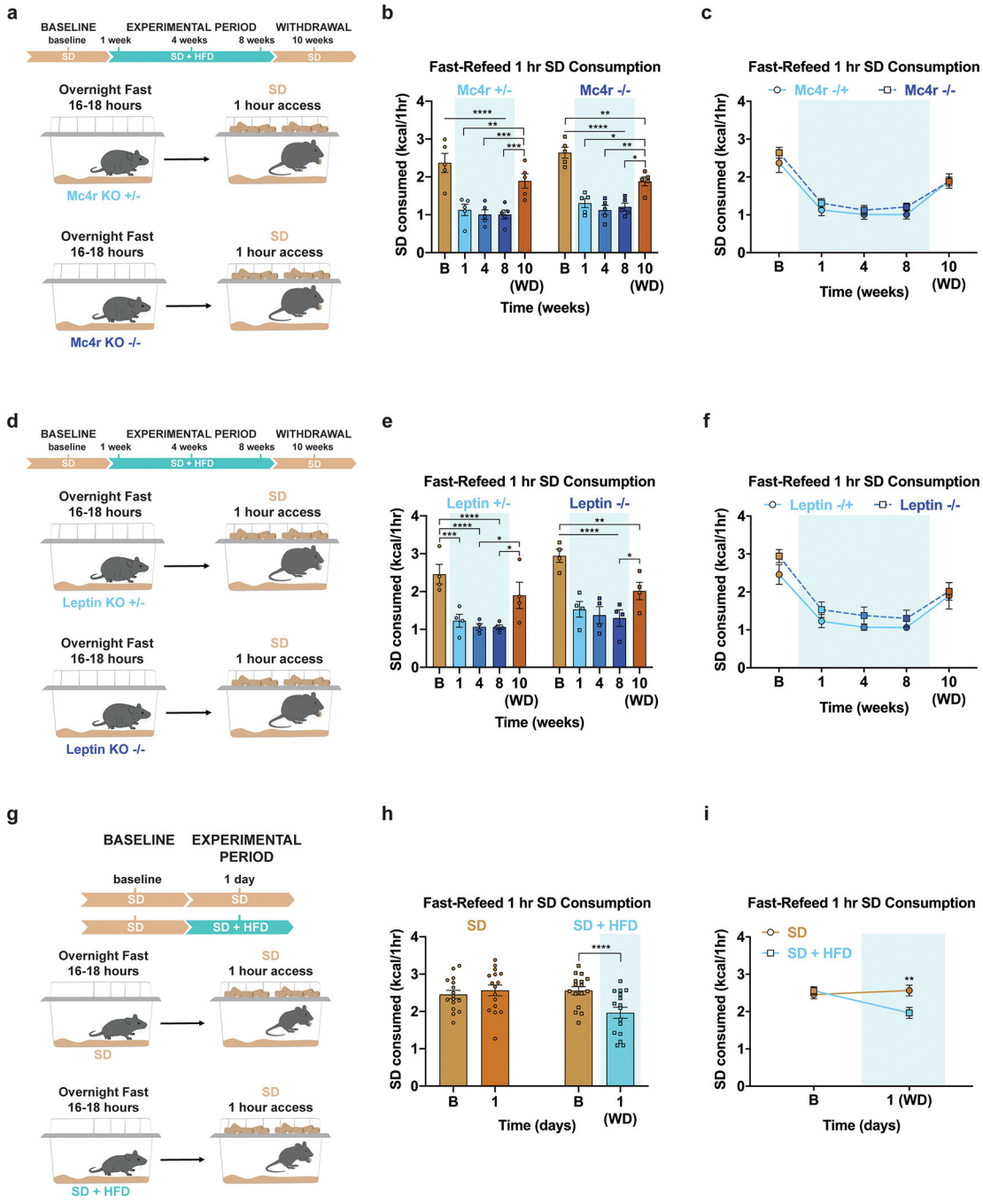

Extended Data Fig. 2: Intact melanocortin-4 receptor- or leptin-signaling are dispensable for SD devaluation following HFD-exposure and 24 hours of HFD-exposure is sufficient to devalue SD.

a,d Experimental timeline and group schematic for fast-refeed test with 1 hr SD access. **b,e** Within-subject and **c,f** between-subject comparisons of 1 hr SD fast-refeed consumption across testing sessions (n=5 per Mc4r KO +/− and −/− group, males and females, RM two-way ANOVA, Time x Group: $F(4, 32) = 0.3173$, $P=0.8643$, Tukey's multiple comparisons) (n=4 per Leptin KO +/− and −/− group, males and females, RM two-way ANOVA, Time x Group: $F(4, 24) = 0.3313$, $P=0.8542$, Tukey's multiple comparisons). **g,** Experimental

timeline and group schematic for fast-refeed test with 1 hr SD access. **h,** Within-subject and **i,** between-subject comparisons of 1 hr SD fast-refeed consumption across testing sessions (n=16 per group, males and females, RM two-way ANOVA, Time x Group: F (1, 30) = 16.96, P=0.0003, Sidak's multiple comparisons test). B=Baseline. WD=withdrawal. Shaded blue area in **b**, **c**, **e**, **f**, **h** and **i** represent HFD homecage availability. All error bars represent s.e.m. $*P < 0.05$, $**P < 0.01$, $***P < 0.001$, $****P < 0.0001$.

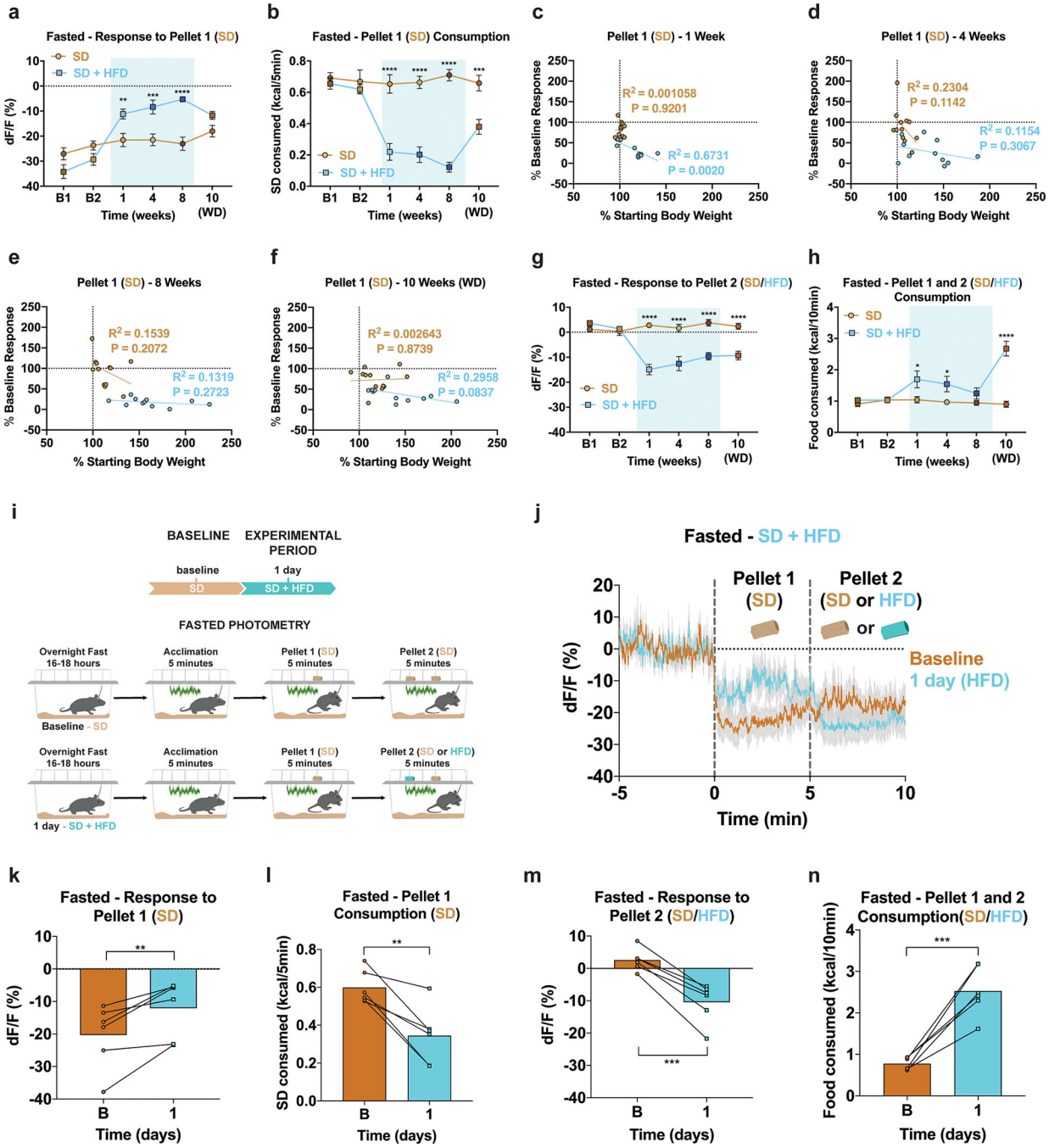

Extended Data Fig. 3: Acute and chronic HFD-exposure alters ARC^{AgRP} activity responses to SD and HFD in fasted mice largely independent of body-weight changes.

a, Between-subject quantification of fasted ARC^{AgRP} activity response to Pellet 1 (SD) (n=12 SD group, n=11 SD + HFD group, males and females, RM two-way ANOVA, Time x Group: F (5, 105) = 16.74, P<0.0001, Bonferroni's multiple comparisons) and **b,** SD consumed across testing sessions (n=12 SD group, n=11 SD + HFD group, males and females, RM two-way ANOVA, Time x Group: F (5, 105) = 15.81, P<0.0001, Bonferroni's multiple comparisons). **c-f,** ARC^{AgRP} activity changes to Pellet 1 (SD) presentation are not strongly correlated with bodyweight accrual over the entire length of the experiment (n=12 SD group, n=11 SD + HFD group, males and females, Linear regression, **c,** SD group: R^2=0.001058, P=0.9201, SD+HFD group: R^2=0.6731, P=0.0020, **d,** SD group: R^2=0.2304, P=0.1142, SD + HFD group: R^2=0.1154, P=0.3067, **e,** SD group: R^2=0.1539, P=0.2072, SD + HFD group: R^2=0.1319, P=0.2723, **f,** SD group: R^2=0.002643, P=0.8739, SD + HFD group: R^2=0.2958, P=0.0837) **g,** Between-subject quantification of fasted ARC^{AgRP} activity response to Pellet 2 (SD for SD group; SD for SD + HFD group during B1 and B2 and HFD for SD + HFD group during 1, 4, 8 and 10 weeks) (n=12 SD group, n=11 SD + HFD group, males and females, RM two-way ANOVA, Time x Group: F (5, 105) = 21.07, P<0.0001, Bonferroni's multiple comparisons) and **h,** total calories consumed across testing sessions (n=12 SD group, n=11 SD + HFD group, males and females, RM two-way ANOVA, Time x Group: F (5, 105) = 14.26, P<0.0001, Bonferroni's multiple comparisons). **i,** Experimental timeline and group schematic for fasted photometry recordings. **j,** Average fasted photometry traces across recording sessions aligned to Pellet 1 and 2 presentation (n=6, males and females). **k,** Within-subject quantification of fasted ARC^{AgRP} activity response to Pellet 1 (SD) (n=6, males and females, Paired t test (two-tailed), P=0.0099) and **l,** SD consumed across testing sessions (n=6, males and females, Paired t test (two-tailed), P=0.0049). **m,** Within-subject quantification of fasted ARC^{AgRP} activity response to Pellet 2 (SD for Baseline; HFD for 1 day) (n=6, males and females, Paired t test (two-tailed), P=0.0008) and **n,** total calories consumed across testing sessions (n=6, males and females, Paired t test (two-tailed), P=0.0008). Shaded blue area in **a-b**, and **g-h** represent HFD homecage availability. B1 and B2 refer to Baseline 1 and 2, respectively. WD=withdrawal. Dotted lines in **j** indicate Pellet 1 and Pellet 2 presentation. All error bars and shaded regions of **j** represent s.e.m. *P < 0.05, **P < 0.01, ***P < 0.001, ****P < 0.0001.

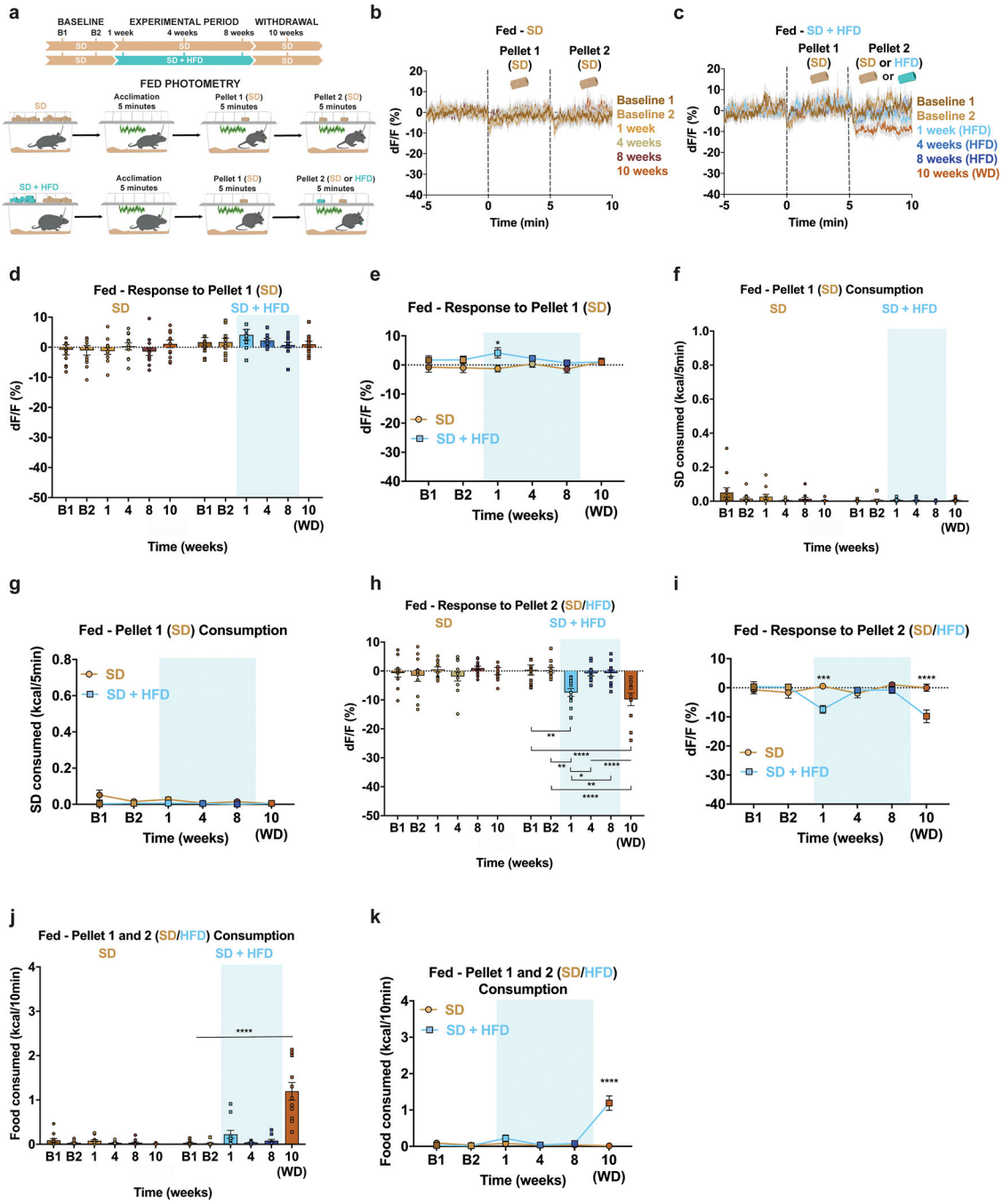

Extended Data Fig. 4: HFD-exposure alters ARC^{AgRP} activity responses to HFD in fed mice.

a, Experimental timeline and group schematic for fed photometry recordings. **b-c,** Average fed photometry traces of the **b,** SD group and **c,** SD + HFD group across recording sessions aligned to Pellet 1 and 2 presentation (n=12 SD group, n=11 SD + HFD group, males and females). **d,** Within- and **e,** between-subject quantification of fed ARC^{AgRP} activity response to Pellet 1 (SD) (n=12 SD group, n=11 SD + HFD group, males and females, RM two-way ANOVA, Time x Group: F (5, 105) = 0.8953, P=0.4872, Bonferroni's multiple comparisons). **f,** Within- and **g,** between-subject quantification of SD consumed across

testing sessions (n=12 SD group, n=11 SD + HFD group, males and females, RM two-way ANOVA, Time x Group: F (5, 105) = 1.768, P=0.1258). **h,** Within- and **i,** between-subject quantification of fed ARC^{AgRP} activity response to Pellet 2 (SD for SD group; SD for SD + HFD group during B1 and B2 and HFD for SD + HFD group during 1, 4, 8 and 10 weeks) (n=12 SD group, n=11 SD + HFD group, males and females, RM two-way ANOVA, Time x Group: F (5, 105) = 7.565, P<0.0001, Bonferroni's multiple comparisons). **j,** Within- and **k,** between-subject quantification of total calories consumed across testing sessions (n=12 SD group, n=11 SD + HFD group, males and females, RM two-way ANOVA, Time x Group: F (5, 105) = 31.68, P<0.0001, Bonferroni's multiple comparisons). Dotted lines in **b,c** indicate Pellet 1 and Pellet 2 presentation. Shaded blue area in **d-k** represent HFD homecage availability. B1 and B2 refer to Baseline 1 and 2, respectively. WD=withdrawal. All error bars and shaded regions of **b-c** represent s.e.m. $*P < 0.05$, $**P < 0.01$, $***P < 0.001$, $****P < 0.0001$.

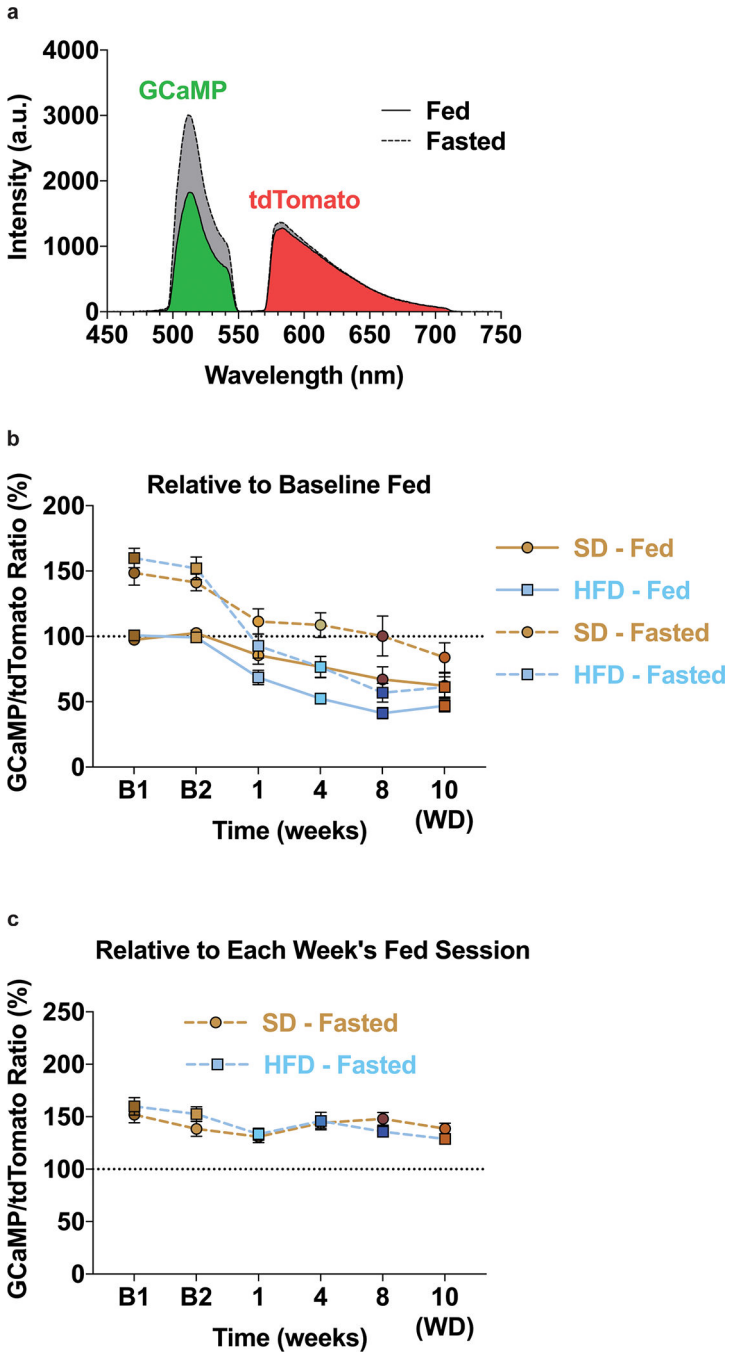

Extended Data Fig. 5: Spectrum-based fiber photometry reveals diminished ARC^{AgRP} baseline activity following HFD exposure.

a, Representative GCaMP and tdTomato emission spectra from a mouse during the Fed and Fasted sessions of Baseline 1 prior to the addition of food. **b,** GCaMP/tdTomato ratios normalized to the mean of Baseline 1+2 Fed values shows basal ARC^{AgRP} activity is increased during Fasted sessions relative to Fed sessions (SD – Fed vs Fasted; HFD – Fed vs Fasted). Homecage HFD exposure reduces basal ARC^{AgRP} activity relative to the SD group across both Fed and Fasted conditions (Fed – SD vs HFD; Fasted – SD vs HFD) (n=12 SD

group, n=11 SD + HFD group, males and females, three-way ANOVA, Diet: $F(1,21) = 6.515$, $P=0.019$, Satiety state: $F(1,63) = 94.128$, $P<0.0001$) **c,** Fasted GCaMP/tdTomato ratios normalized to the Fed values across recording sessions demonstrates an ~50% fasting-induced increase in the GCaMP/tdTomato ratio across all recording weeks (n=12 SD group, n=11 SD + HFD group, males and females, RM two-way ANOVA, Time x Group: $F(5, 105) = 1.978$, $P=0.0879$). B1 and B2 refer to Baseline 1 and 2, respectively. WD=withdrawal.

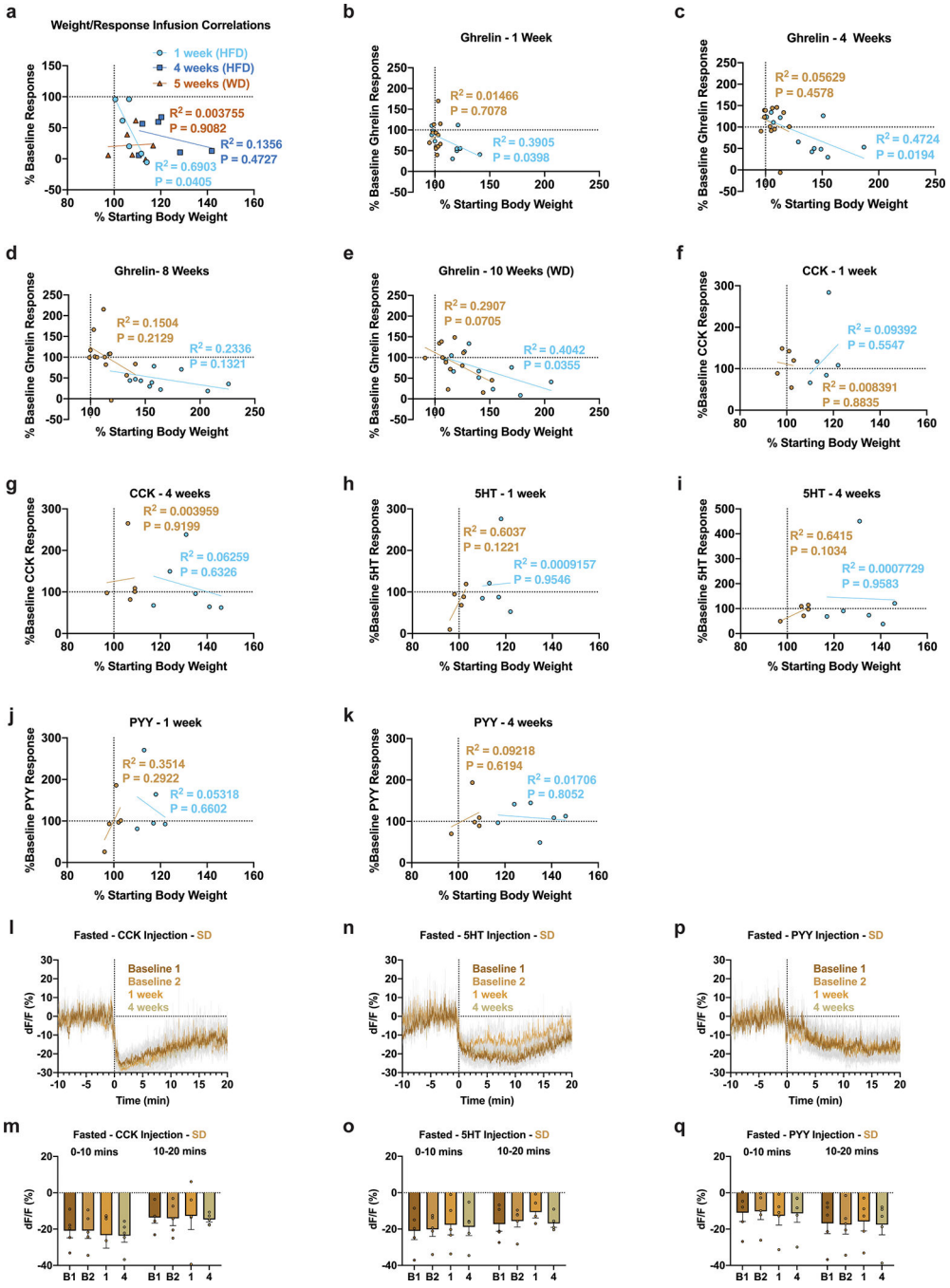

Extended Data Fig. 6: Physiological disruption of ARC^{AgRP} activity in response to HFD-exposure is partially dependent on body weight gain.

a, Changes in ARC^{AgRP} activity in response to identical caloric load is correlated to weight gain 1, but not 4 weeks after HFD exposure or 1 week HFD withdrawal (n=6, males and females, Linear regression, 1 week (HFD): R^2=0.6903, P=0.0405, 4 weeks (HFD): R^2=0.1356, P=0.4727, 5 weeks (WD): R^2=0.003755, P=0.9082). **b-e,** Changes in ARC^{AgRP} activity in response to ghrelin is correlated to weight gain (n=12 SD group, n=11 SD + HFD group, males and females, Linear regression, **b,** SD group: R^2=0.01466, P=0.7078, SD +HFD group: R^2=0.3905, P=0.0398, **c,** SD group: R^2=0.05629, P=0.4578, SD+HFD group: R^2=0.4724, P=0.0194, **d,** SD group: SD group: R^2=0.1504, P=0.2129, SD+HFD group: R^2=0.2336, P=0.1321), **e,** SD group: R^2=0.2907, P=0.0705, SD+HFD group: R^2=0.4042, P=0.0355. **f-k,** Changes in ARC^{AgRP} activity in response to **f-g,** CCK, **h-I,** 5HT or **j-k,** PYY is not correlated to weight gain (n=5 SD group, n=6 SD + HFD group, males and females, Linear regression, **f,** SD group: R^2=0.008391, P=0.8835, SD+HFD group: R^2=0.09392, P=0.5547, **g,** SD group: R^2=0.003959, P=0.9199, SD+HFD group: R^2=0.06259, P=0.6326, **h,** SD group: R^2=0.6037, P=0.1221, SD+HFD group: R^2=0.0009157, P=0.9546, **i,** SD group: R^2=0.6415, P=0.1034, SD+HFD group: R^2=0.0007729, P=0.9583, **j,** SD group: R^2=0.3514, P=0.2922, SD+HFD group: R^2=0.05138, P=0.6602, **k,** SD group: R^2=0.09218, P=0.6194, SD+HFD group: R^2=0.01706, P=0.8052). **l,n,p,** Average photometry traces of the SD group across recording sessions aligned to **l,** CCK, **n,** 5HT or **p,** PYY injection (n=5 SD group, males and females). **m,o,q,** Within-subject quantification of ARC^{AgRP} activity to **m,** CCK (n=5 SD group, males and females, RM two-way ANOVA, Time Bin x Week: F (1.511, 6.045) = 1.014, P=0.3923), **o,** 5HT (n=5 SD group, males and females, RM two-way ANOVA, Time Bin x Week: F (2.334, 9.337) = 1.242, P=0.3393) or **q,** PYY (n=5 SD group, males and females, RM two-way ANOVA, Time Bin x Week: F (1.897, 7.589) = 1.885, P=0.2164) across testing sessions. Dotted lines indicate **l,** CCK, **n,** 5HT or **p,** PYY injection. B1 and B2 refer to Baseline 1 and 2, respectively. All error bars and shaded regions of **l,n,** and **p** represent s.e.m.

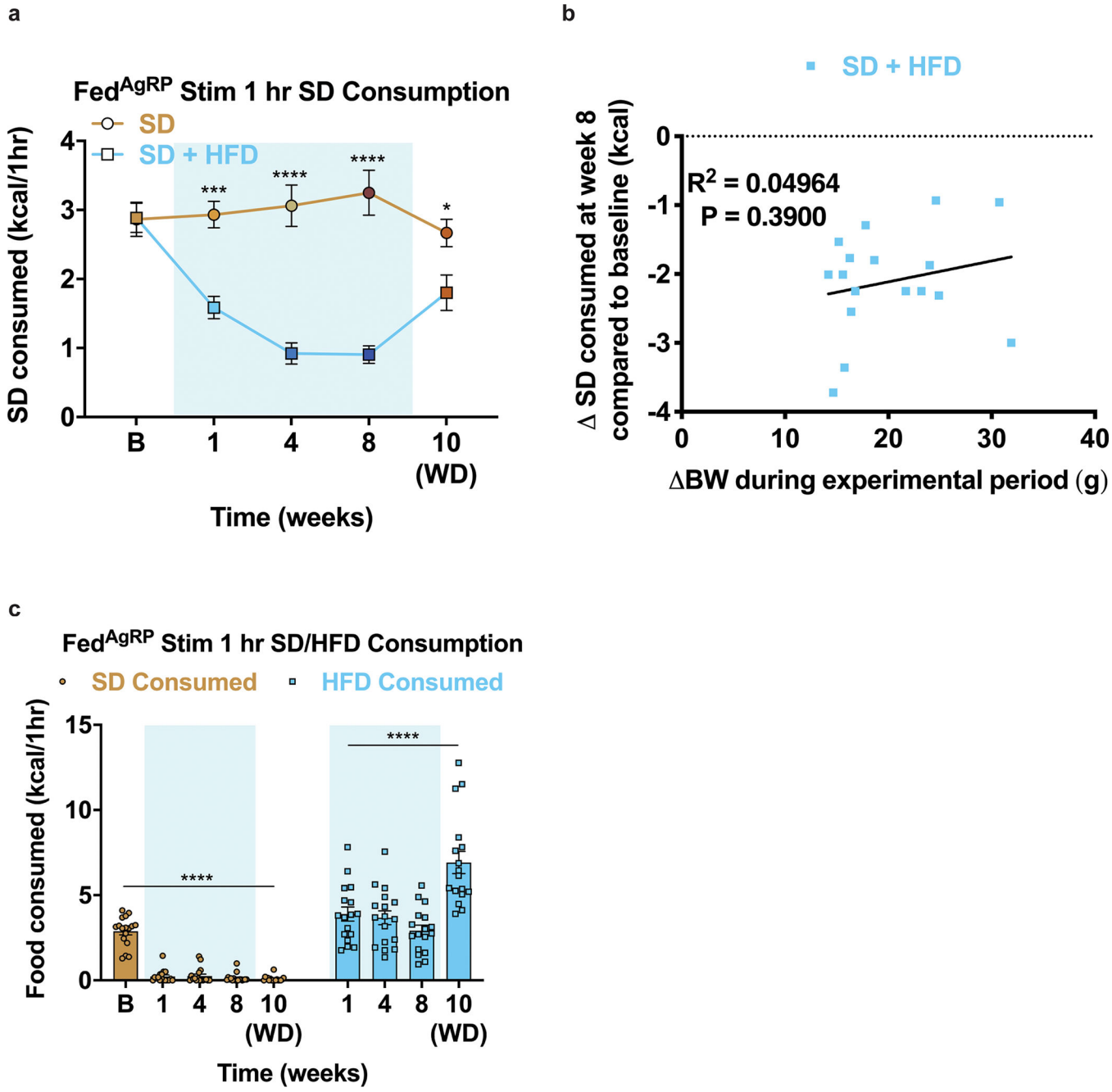

Extended Data Fig. 7: HFD exposure promotes devaluation of optogenetic ARC^{AgRP}-evoked SD, but not HFD, and consumption independent of weight gain.

a, Between-subject comparison of fed^{AgRP} stimulation 1 hr SD consumption across test sessions (n=16 SD group, n=17 SD + HFD group, males and females, RM two-way ANOVA, Time x Group: F (4, 124) = 18.85, P<0.0001, Bonferroni's multiple comparisons). **b,** No correlation between SD devaluation at Week 8 relative to Baseline and body weight changes after 8 weeks of access to SD and HFD (n=17, males and females, Linear regression, R^2=0.04964, P=0.3900). **c,** Within-subject, within-diet comparisons of fed^{AgRP} stimulation 1 hr SD and HFD consumption across testing sessions (n=17, males and

females, RM one-way ANOVAs, Tukey's multiple comparisons). B=Baseline. WD=Withdrawal. Shaded blue area in **a** and **c** represent HFD homecage availability. All error bars represent s.e.m. *$P < 0.05$, **$P < 0.01$, ***$P < 0.001$, ****$P < 0.0001$.

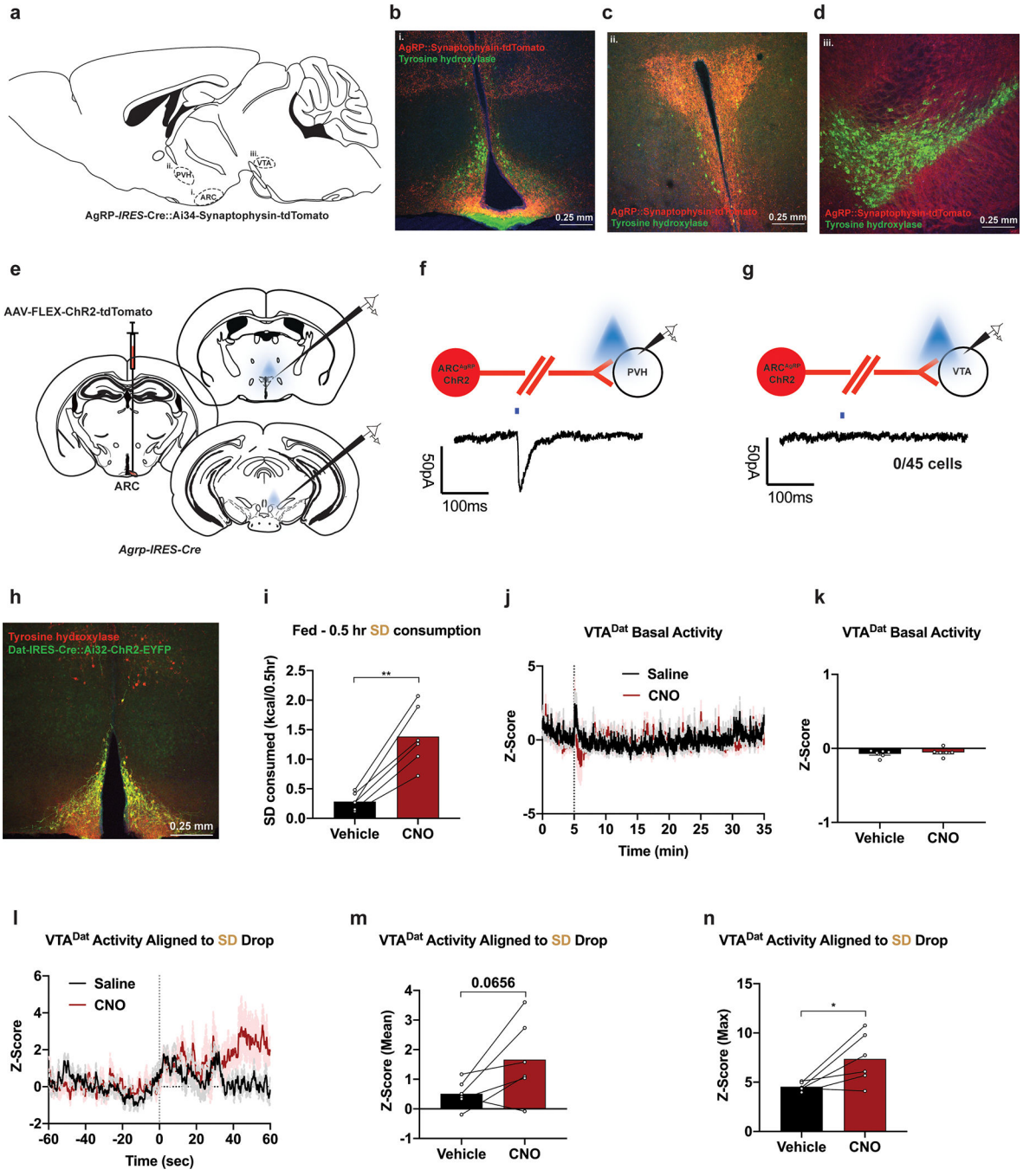

Extended Data Fig. 8: ARC$^{AgRP/Npy}$ activation does not alter basal VTA^{Dat} activity but potentiates signaling in response to food via an indirect signaling mechanism.

a, Brain schematic of anterograde tracing strategy. **b-d,** representative images of AgRP::Synaptophysin-tdTomato and tyrosine hydroxylase (TH) in the **b,** arcuate nucleus, **c,** paraventricular hypothalamus and **d,** ventral tegmental area. **e,** Brain schematic of unilateral

viral delivery of Cre-inducible ChR2 to the ARC of AgRP-ires-Cre mice and position of ex vivo slice recordings from PVH (top) and VTA (bottom) cells. **f-g,** ChR2-assisted circuit mapping schematic and representative trace from **f,** PVH and **g**, VTA cells. **h,** Representative image of Dat-ires-Cre::Ai32-ChR2-eYFP and overlap with TH in the ARC. **i,** Chemogenetic ARC^{Npy} activation drives food intake (n=6, males and females, Paired t test (two-tailed), P=0.0013). **j,** Averaged Z-score traces and **k,** quantification of basal VTA^{Dat} activity after saline or CNO injections (n=6, males and females, Paired t test (two-tailed), P=0.2837). **l,** Averaged Z-score traces and **m,** mean (n=6, males and females, Paired t test (two-tailed), P=0.0656) and **n,** max quantification (n=6, males and females, Paired t test (two-tailed), P=0.0365) of VTA^{Dat} activity in response to SD food drop after saline or CNO injections. All error bars represent s.e.m. $*P < 0.05$, $**P < 0.01$.

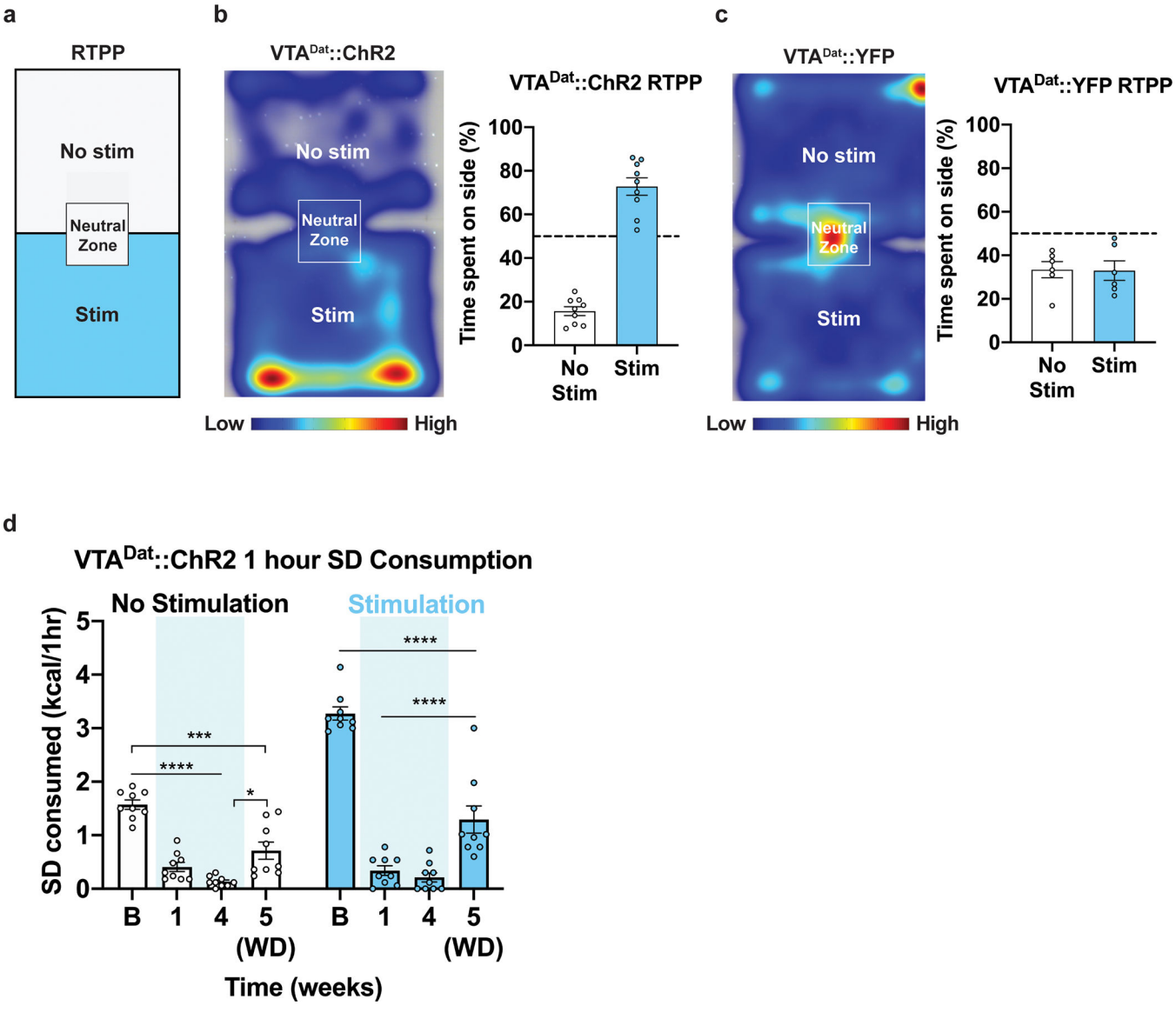

Extended Data Fig. 9: VTA^{Dat} photostimulation is intrinsically rewarding but loses the capacity to enhance SD consumption in fasted mice after HFD exposure.

a, Schematic of Real-Time Place Preference assay. **b,** Averaged heat maps and quantification of time spent in each chamber of the RTPP assay in VTA^{Dat}::ChR2 mice (n=9, males, Paired t test (two-tailed), P<0.0001). c, Averaged heat maps and quantification of time spent in each chamber of the RTPP assay in control VTA^{Dat}::YFP mice (n=6, males, Paired t test (two-tailed), P=0.9576). **d,** Within-subject and condition comparisons of 1 hr SD consumption across testing sessions with or without VTA^{Dat} photostimulation (n=9, males, RM two-way ANOVA, Time x Condition: F (3, 48) = 18.30, P<0.0001, Tukey's multiple comparisons). B=Baseline. WD=Withdrawal. Shaded blue area in **d** represents HFD homecage availability. All error bars represent s.e.m. ***$P < 0.001$, ****$P < 0.0001$.

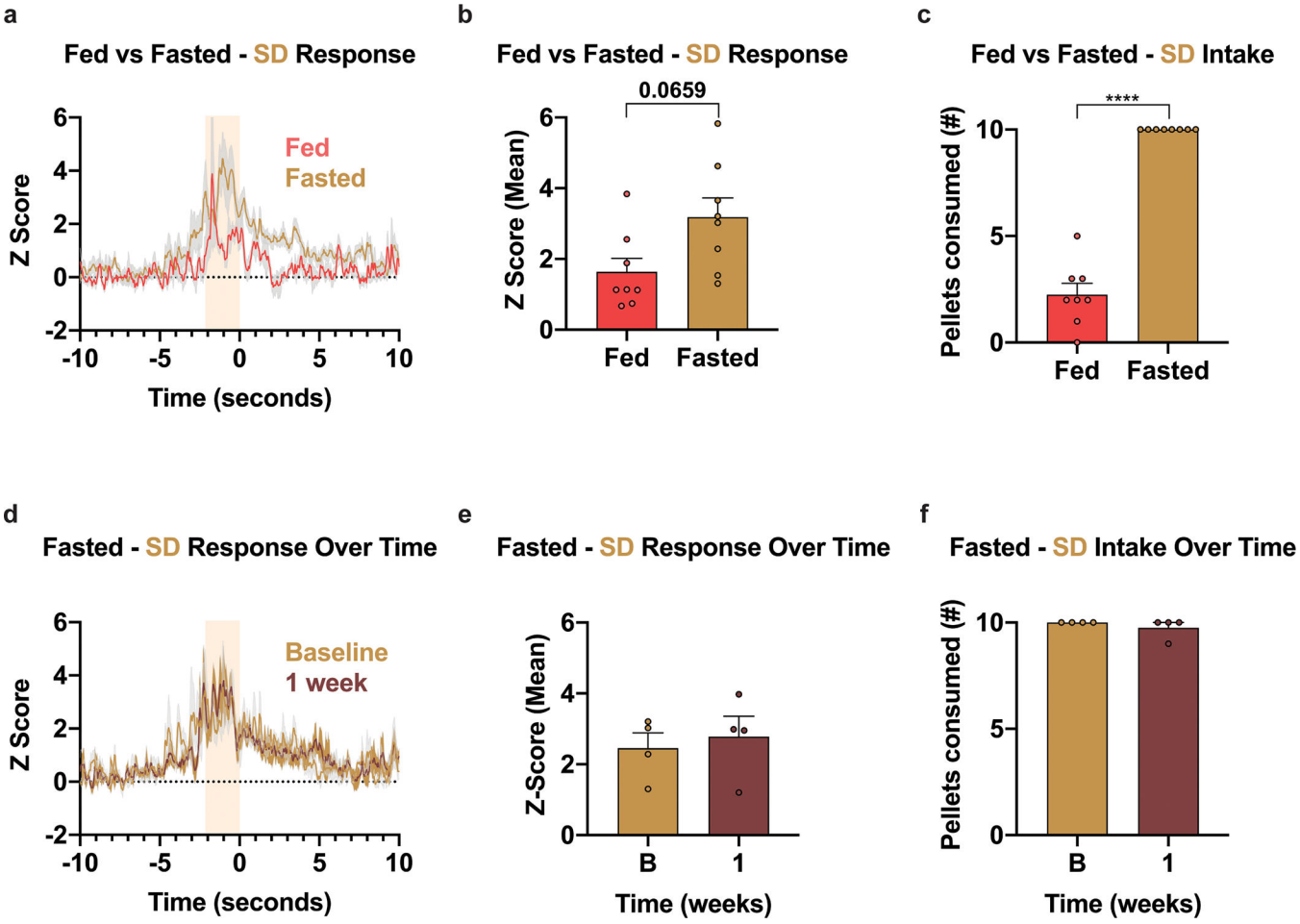

Extended Data Fig. 10: DA responses to SD are state-dependent and consistent over time in HFD-naïve animals.

a, Averaged Z-score traces of DA2m fluorescence aligned to SD pellet retrieval across appetite state (n=8, males and females). **b,** Within-subject comparisons of mean fluorescence Z-score during SD pellet retrieval across appetite state (n=8, males and females, Paired t test (two-tailed), P=0.0659). **c,** Within-subject comparisons of SD pellets consumed across appetite state (n=8, males and females, Paired t test (two-tailed), P<0.0001). **d,** Averaged Z-score traces of DA2m fluorescence aligned to SD pellet retrieval across recording weeks. (n=4, males and females) **e,** Within-subject comparisons of mean fluorescence Z-score

during SD pellet retrieval across sessions (n=4, males and females, Wilcoxon matched-pairs signed rank test, P=0.625). **f,** Within-subject comparisons of SD pellets consumed across sessions (n=4, males and females, Wilcoxon matched-pairs signed rank test, P>0.9999). Time 0 denotes consumption. B=Baseline. Shaded peach region in **a** and **d** represent quantified pellet approach/retrieval period. All error bars and shaded regions of **a** and **d** represent s.e.m. ****$P < 0.0001$.

Supplementary Material

Refer to Web version on PubMed Central for supplementary material.

Acknowledgments

Research was supported by an NIEHS-NIDDK joint fellowship. We thank Dr. N. Martin and Dr. B. Gloss of the NIEHS Viral Vector Core for producing AAVs and J. Tucker of the NIEHS Fluorescence Microscopy and Imaging Center for assistance with image acquisition. We thank the GENIE project for the development of GCaMP6. We would also like to thank all lab members of Dr. Krashes' and Dr. Cui's lab for their technical support and guidance throughout this work, and Dr. J. Cushman of the NIEHS Neurobehavioral Core for assistance with behavioral studies and statistical analyses. This work was supported by the Intramural Research Program of the NIH, the National Institute of Environmental Health Sciences—NIEHS: 1ZIAES103310 (to G.C.), the National Institutes of Diabetes and Digestive and Kidney Diseases—NIDDK: DK075088 (to M.J.K.), DK075087-06 (to M.J.K.), NIEHS-NIDDK Joint Fellowship Award (to C.M.M.) and the Center of Compulsive Behaviors (to C.M.M. and I.D.A.S.).

References

1. Timper K & Brüning JC Hypothalamic circuits regulating appetite and energy homeostasis: pathways to obesity. Dis. Model. Mech 10, 679–689 (2017). [PubMed: 28592656]
2. DiFeliceantonio AG & Small DM Dopamine and diet-induced obesity. Nat. Neurosci 22, 1–2 (2019). [PubMed: 30559474]
3. Ferrario CR et al. Homeostasis Meets Motivation in the Battle to Control Food Intake. J. Neurosci 36, 11469–11481 (2016). [PubMed: 27911750]
4. Luquet S, Perez FA, Hnasko TS & Palmiter RD NPY/AgRP neurons are essential for feeding in adult mice but can be ablated in neonates. Science 310, 683–5 (2005). [PubMed: 16254186]
5. Aponte Y, Atasoy D & Sternson SM AGRP neurons are sufficient to orchestrate feeding behavior rapidly and without training. Nat. Neurosci 14, 351–355 (2011). [PubMed: 21209617]
6. Krashes MJ et al. Rapid, reversible activation of AgRP neurons drives feeding behavior in mice. J. Clin. Invest 121, 1424–1428 (2011). [PubMed: 21364278]
7. Takahashi KA & Cone RD Fasting Induces a Large, Leptin-Dependent Increase in the Intrinsic Action Potential Frequency of Orexigenic Arcuate Nucleus Neuropeptide Y/Agouti-Related Protein Neurons. Endocrinology 146, 1043–1047 (2005). [PubMed: 15591135]
8. Mandelblat-Cerf Y et al. Arcuate hypothalamic AgRP and putative pomc neurons show opposite changes in spiking across multiple timescales. Elife 4, 1–25 (2015).
9. Chen Y, Lin Y-C, Kuo T-W & Knight ZA Sensory Detection of Food Rapidly Modulates Arcuate Feeding Circuits. Cell 160, 829–841 (2015). [PubMed: 25703096]
10. Beutler LR et al. Dynamics of Gut-Brain Communication Underlying Hunger. Neuron 96, 461–475.e5 (2017). [PubMed: 29024666]
11. Su Z, Alhadeff AL & Betley JN Nutritive, Post-ingestive Signals Are the Primary Regulators of AgRP Neuron Activity. Cell Rep. 21, 2724–2736 (2017). [PubMed: 29212021]
12. Betley JN et al. Neurons for hunger and thirst transmit a negative-valence teaching signal. Nature 521, 180–185 (2015). [PubMed: 25915020]
13. Baver SB et al. Leptin modulates the intrinsic excitability of AgRP/NPY neurons in the arcuate nucleus of the hypothalamus. J. Neurosci 34, 5486–96 (2014). [PubMed: 24741039]

14. Salamone JD, Correa M, Mingote S & Weber SM Nucleus accumbens dopamine and the regulation of effort in food-seeking behavior: implications for studies of natural motivation, psychiatry, and drug abuse. J. Pharmacol. Exp. Ther 305, 1–8 (2003). [PubMed: 12649346]
15. Berridge KC 'Liking' and 'wanting' food rewards: Brain substrates and roles in eating disorders. Physiol. Behav 97, 537–550 (2009). [PubMed: 19336238]
16. Wise RA Role of brain dopamine in food reward and reinforcement. Philos. Trans. R. Soc. B Biol. Sci 361, 1149–1158 (2006).
17. Alhadeff AL et al. Natural and Drug Rewards Engage Distinct Pathways that Converge on Coordinated Hypothalamic and Reward Circuits. Neuron 103, 891–908.e6 (2019). [PubMed: 31277924]
18. Denis RGP et al. Palatability Can Drive Feeding Independent of AgRP Neurons. Cell Metab. 22, 646–657 (2015). [PubMed: 26278050]
19. Fordahl SC & Jones SR High-Fat-Diet-Induced Deficits in Dopamine Terminal Function Are Reversed by Restoring Insulin Signaling. ACS Chem. Neurosci 8, 290–299 (2017). [PubMed: 27966885]
20. Rothemund Y et al. Differential activation of the dorsal striatum by high-calorie visual food stimuli in obese individuals. Neuroimage 37, 410–421 (2007). [PubMed: 17566768]
21. Stice E, Spoor S, Bohon C, Veldhuizen MG & Small DM Relation of reward from food intake and anticipated food intake to obesity: a functional magnetic resonance imaging study. J. Abnorm. Psychol 117, 924–35 (2008). [PubMed: 19025237]
22. Thanarajah SE et al. Food Intake Recruits Orosensory and Post-ingestive Dopaminergic Circuits to Affect Eating Desire in Humans. Cell Metab. 29, 695–706.e4 (2019). [PubMed: 30595479]
23. Ravussin Y et al. Effects of chronic weight perturbation on energy homeostasis and brain structure in mice. Am. J. Physiol. Integr. Comp. Physiol 300, R1352–R1362 (2011).
24. Johnson PM & Kenny PJ Dopamine D2 receptors in addiction-like reward dysfunction and compulsive eating in obese rats. Nat. Neurosci 13, 635–641 (2010). [PubMed: 20348917]
25. Cone JJ, Chartoff EH, Potter DN, Ebner SR & Roitman MF Prolonged High Fat Diet Reduces Dopamine Reuptake without Altering DAT Gene Expression. PLoS One 8, e58251 (2013). [PubMed: 23516454]
26. Drewnowski A & Greenwood MRC Cream and sugar: Human preferences for high-fat foods. Physiol. Behav 30, 629–633 (1983). [PubMed: 6878464]
27. Yang Y, Jr DLS, Keating KD, Allison DB & Nagy TR Variations in Body Weight, Food Intake and Body Composition after Long-Term High-Fat Diet Feeding in C57BL / 6J Mice. 22, 2147–2155 (2014).
28. Guo J, Jou W, Gavrilova O & Hall KD Persistent diet-induced obesity in male C57BL/6 mice resulting from temporary obesigenic diets. PLoS One 4, (2009).
29. Carlin JL et al. Removal of high-fat diet after chronic exposure drives binge behavior and dopaminergic dysregulation in female mice. Neuroscience 326, 170–179 (2016). [PubMed: 27063418]
30. Balthasar N et al. Divergence of Melanocortin Pathways in the Control of Food Intake and Energy Expenditure. Cell 123, 493–505 (2005). [PubMed: 16269339]
31. Zhang Y et al. Positional cloning of the mouse obese gene and its human homologue. Nature 372, 425–32 (1994). [PubMed: 7984236]
32. Jais A & Brüning JC Hypothalamic inflammation in obesity and metabolic disease. J. Clin. Invest 127, 24–32 (2017). [PubMed: 28045396]
33. Chen T-W et al. Ultrasensitive fluorescent proteins for imaging neuronal activity. Nature 499, 295–300 (2013). [PubMed: 23868258]
34. Garfield AS et al. Dynamic GABAergic afferent modulation of AgRP neurons. Nat. Neurosci 19, 1628–1635 (2016). [PubMed: 27643429]
35. Hahn TM, Breininger JF, Baskin DG & Schwartz MW Coexpression of Agrp and NPY in fasting-activated hypothalamic neurons. Nat. Neurosci 1, 271–272 (1998). [PubMed: 10195157]

36. Briggs DI, Enriori PJ, Lemus MB, Cowley MA & Andrews ZB Diet-Induced Obesity Causes Ghrelin Resistance in Arcuate NPY/AgRP Neurons. Endocrinology 151, 4745–4755 (2010). [PubMed: 20826561]

37. Briggs DI et al. Calorie-restricted weight loss reverses high-fat diet-induced ghrelin resistance, which contributes to rebound weight gain in a ghrelin-dependent manner. Endocrinology 154, 709–717 (2013). [PubMed: 23307790]

38. Liu S et al. Consumption of palatable food primes food approach behavior by rapidly increasing synaptic density in the VTA. Proc. Natl. Acad. Sci 113, 2520–2525 (2016). [PubMed: 26884159]

39. Roitman MF, Stuber GD, Phillips PEM, Wightman RM & Carelli RM Dopamine operates as a subsecond modulator of food seeking. J. Neurosci 24, 1265–71 (2004). [PubMed: 14960596]

40. Atasoy D, Aponte Y, Su HH & Sternson SM A FLEX Switch Targets Channelrhodopsin-2 to Multiple Cell Types for Imaging and Long-Range Circuit Mapping. J. Neurosci 28, 7025–7030 (2008). [PubMed: 18614669]

41. Armbruster BN, Li X, Pausch MH, Herlitze S & Roth BL Evolving the lock to fit the key to create a family of G protein-coupled receptors potently activated by an inert ligand. Proc. Natl. Acad. Sci. U. S. A 104, 5163–8 (2007). [PubMed: 17360345]

42. Alexander GM et al. Remote control of neuronal activity in transgenic mice expressing evolved G protein-coupled receptors. Neuron 63, 27–39 (2009). [PubMed: 19607790]

43. Tsai H-C et al. Phasic firing in dopaminergic neurons is sufficient for behavioral conditioning. Science 324, 1080–4 (2009). [PubMed: 19389999]

44. Sun F et al. A Genetically Encoded Fluorescent Sensor Enables Rapid and Specific Detection of Dopamine in Flies, Fish, and Mice. Cell 174, 481–496.e19 (2018). [PubMed: 30007419]

45. Betley JN, Cao ZFH, Ritola KD & Sternson SM Parallel, Redundant Circuit Organization for Homeostatic Control of Feeding Behavior. Cell 155, 1337–1350 (2013). [PubMed: 24315102]

46. Lippert RN et al. Maternal high-fat diet during lactation reprograms the dopaminergic circuitry in mice. J. Clin. Invest (2020). doi:10.1172/JCI134412

47. Tellez LA et al. Separate circuitries encode the hedonic and nutritional values of sugar. Nat. Neurosci 19, 465–470 (2016). [PubMed: 26807950]

48. Stice E, Yokum S, Blum K & Bohon C Weight Gain Is Associated with Reduced Striatal Response to Palatable Food. J. Neurosci 30, 13105–13109 (2010). [PubMed: 20881128]

49. Volkow ND, Wang G-J & Baler RD Reward, dopamine and the control of food intake: implications for obesity. Trends Cogn. Sci 15, 37–46 (2011). [PubMed: 21109477]

References in Methods

50. Madisen L et al. A robust and high-throughput Cre reporting and characterization system for the whole mouse brain. Nat. Neurosci 13, 133–40 (2010). [PubMed: 20023653]

51. Meng C et al. Spectrally Resolved Fiber Photometry for Multi-component Analysis of Brain Circuits. Neuron 98, 707–717.e4 (2018). [PubMed: 29731250]

52. Nguyen KP, O'Neal TJ, Bolonduro OA, White E & Kravitz AV Feeding Experimentation Device (FED): A flexible open-source device for measuring feeding behavior. J. Neurosci. Methods 267, 108–114 (2016). [PubMed: 27060385]

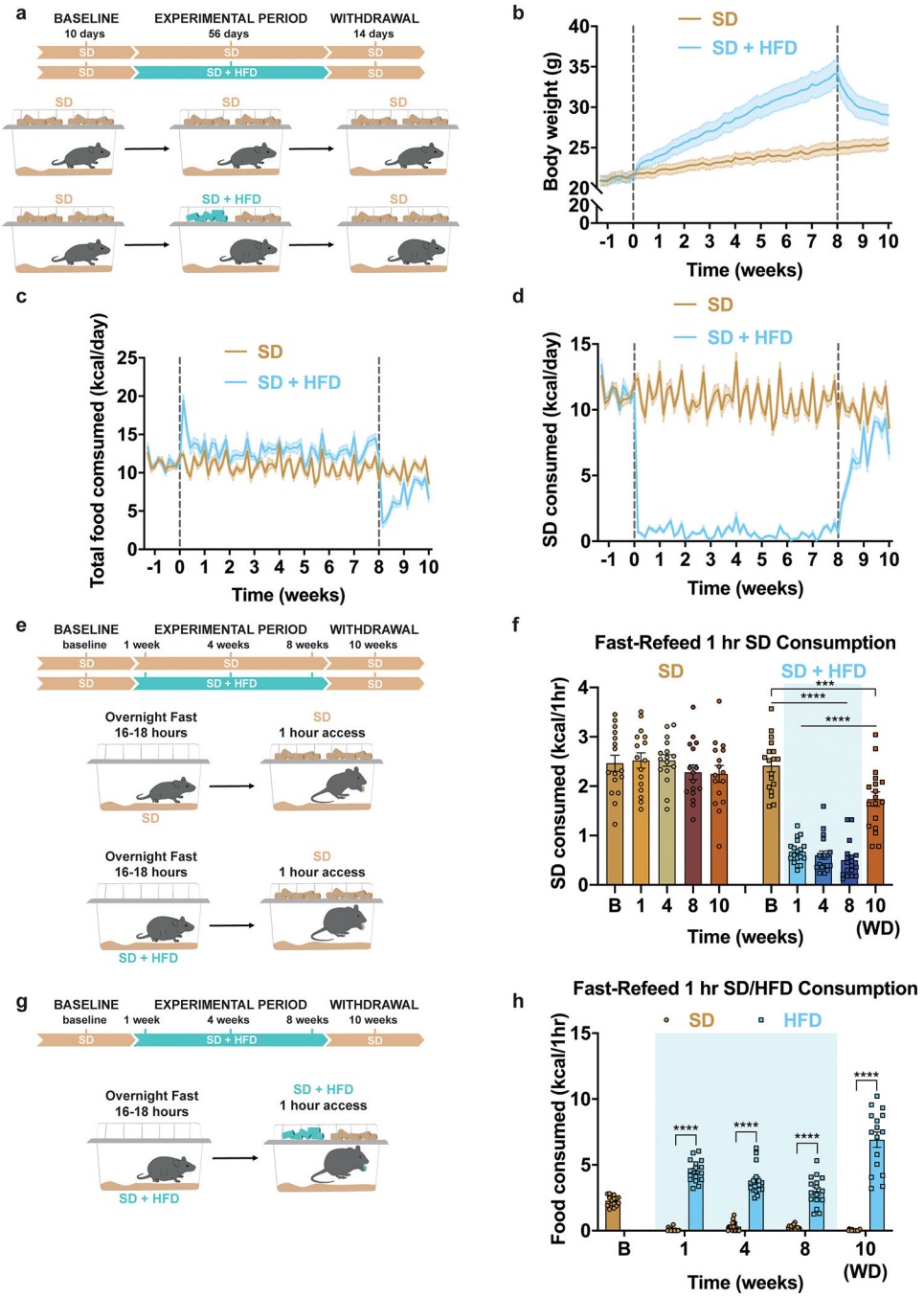

Figure 1: HFD-exposure promotes weight gain and devaluation of SD.

a, Experimental timeline and group schematic for home cage measurements. Daily **b,** body weight (n=20 per group, males and females, RM two-way ANOVA, Day x Group: F (79, 3002) = 33.34, P<0.0001) **c,** total food intake (n=20 per group, males and females, RM two-way ANOVA, Day x Group: F (79, 3002) = 18.73, P<0.0001) and **d,** SD intake throughout the duration of the experiment (n=20 per group, males and females, RM two-way ANOVA, Day x Group: F (79, 3002) = 95.76, P<0.0001). **e,** Experimental timeline and group schematic for fast-refeed test with 1 hr SD access. **f,** Within-subject comparison of 1 hr SD

fast-refeed consumption across testing sessions (n=16 SD group, n=18 SD + HFD group, males and females, RM two-way ANOVA, Time x Group: F (4, 128) = 28.99, P<0.0001, Tukey's multiple comparisons). **g,** Experimental timeline and group schematic for fast-refeed test with 1 hr SD and HFD access. **h,** Within-subject comparison of 1 hr SD and HFD fast-refeed consumption across testing sessions (n=16, males and females, RM two-way ANOVA, Time x Diet: F (3, 90) = 30.58, P<0.0001, Tukey's multiple comparisons). Dotted lines in **b, c, d** delineate window of HFD availability. B=Baseline. WD=withdrawal. Shaded blue area in **f** and **h** represent HFD homecage availability. All error bars and shaded regions of **b, c,** and **d** represent mean ± s.e.m. ***$P < 0.001$, ****$P < 0.0001$.

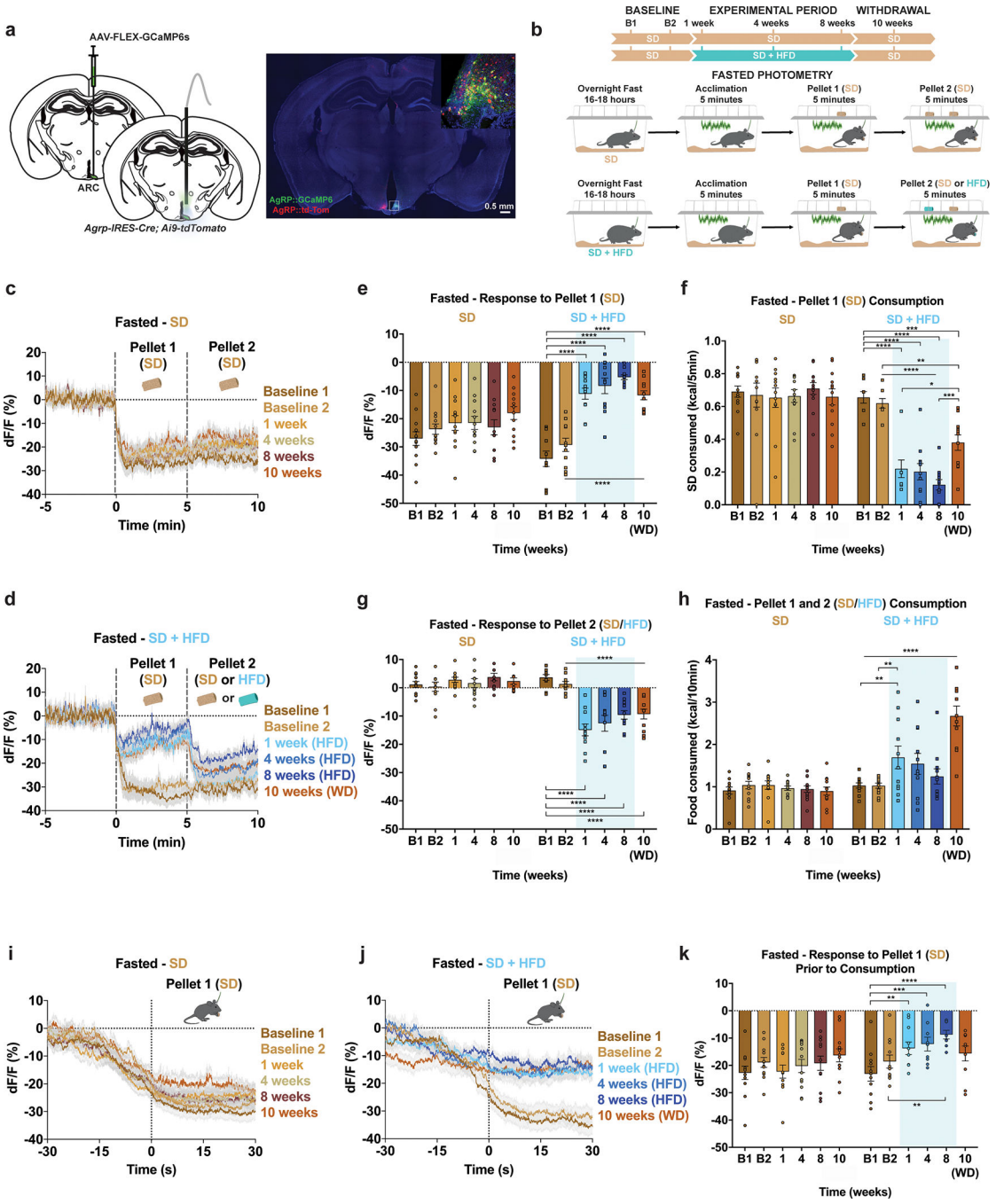

Figure 2: HFD-exposure alters ARC^{AgRP} activity responses to SD and HFD in fasted mice.

a, Left, Brain schematic of unilateral viral delivery of Cre-inducible GCaMP6s to the ARC of AgRP-ires-Cre; Ai9-tdTomato reporter mice and optical fiber implant. Right, representative image of GCaMP6s and tdTomato expression. **b,** Experimental timeline and group schematic for fasted photometry recordings. **c-d,** Average fasted photometry traces of the **c,** SD group and **d,** SD + HFD group across recording sessions aligned to Pellet 1 and 2 presentation (n=12 SD group, n=11 SD + HFD group, males and females). **e,** Within-subject quantification of fasted ARC^{AgRP} activity response to Pellet 1 (SD) (n=12 SD group, n=11

SD + HFD group, males and females, RM two-way ANOVA, Time x Group: F (5, 105) = 16.74, P<0.0001, Bonferroni's multiple comparisons). and **f,** SD consumed across testing sessions during the first 5 minutes of food access (n=12 SD group, n=11 SD + HFD group, males and females, RM two-way ANOVA, Time x Group: F (5, 105) = 15.81, P<0.0001, Bonferroni's multiple comparisons). **g,** Within-subject quantification of fasted ARC^{AgRP} activity response to Pellet 2 (SD for SD group; SD for SD + HFD group during B1 and B2 and HFD for SD + HFD group during 1, 4, 8 and 10 weeks) (n=12 SD group, n=11 SD + HFD group, males and females, RM two-way ANOVA, Time x Group: F (5, 105) = 21.07, P<0.0001, Bonferroni's multiple comparisons) and **h,** total calories consumed across testing sessions (n=12 SD group, n=11 SD + HFD group, males and females, RM two-way ANOVA, Time x Group: F (5, 105) = 14.26, P<0.0001, Bonferroni's multiple comparisons). **i-j,** Average fasted photometry traces of the **i,** SD group and **j,** SD + HFD group across recording sessions aligned to Pellet 1 (SD) consumption. **k,** Within-subject quantification of fasted ARC^{AgRP} activity response to Pellet 1 (SD) consumption (n=12 SD group, n=8–11 SD + HFD group, males and females, Mixed-effects model (REML), Time x Group: F (5, 99) = 3.735, P=0.0039, Bonferroni's multiple comparisons). Dotted lines in **c,d** indicate Pellet 1 and Pellet 2 presentation. Dotted lines in **i,j** indicate Pellet 1 consumption. Shaded blue area in **e-h**, and **k** represent HFD homecage availability. B1 and B2 refer to Baseline 1 and 2, respectively. WD=withdrawal. All error bars and shaded regions of **c-d** and **i-j** represent s.e.m. $*P < 0.05$, $**P < 0.01$, $***P < 0.001$, $****P < 0.0001$.

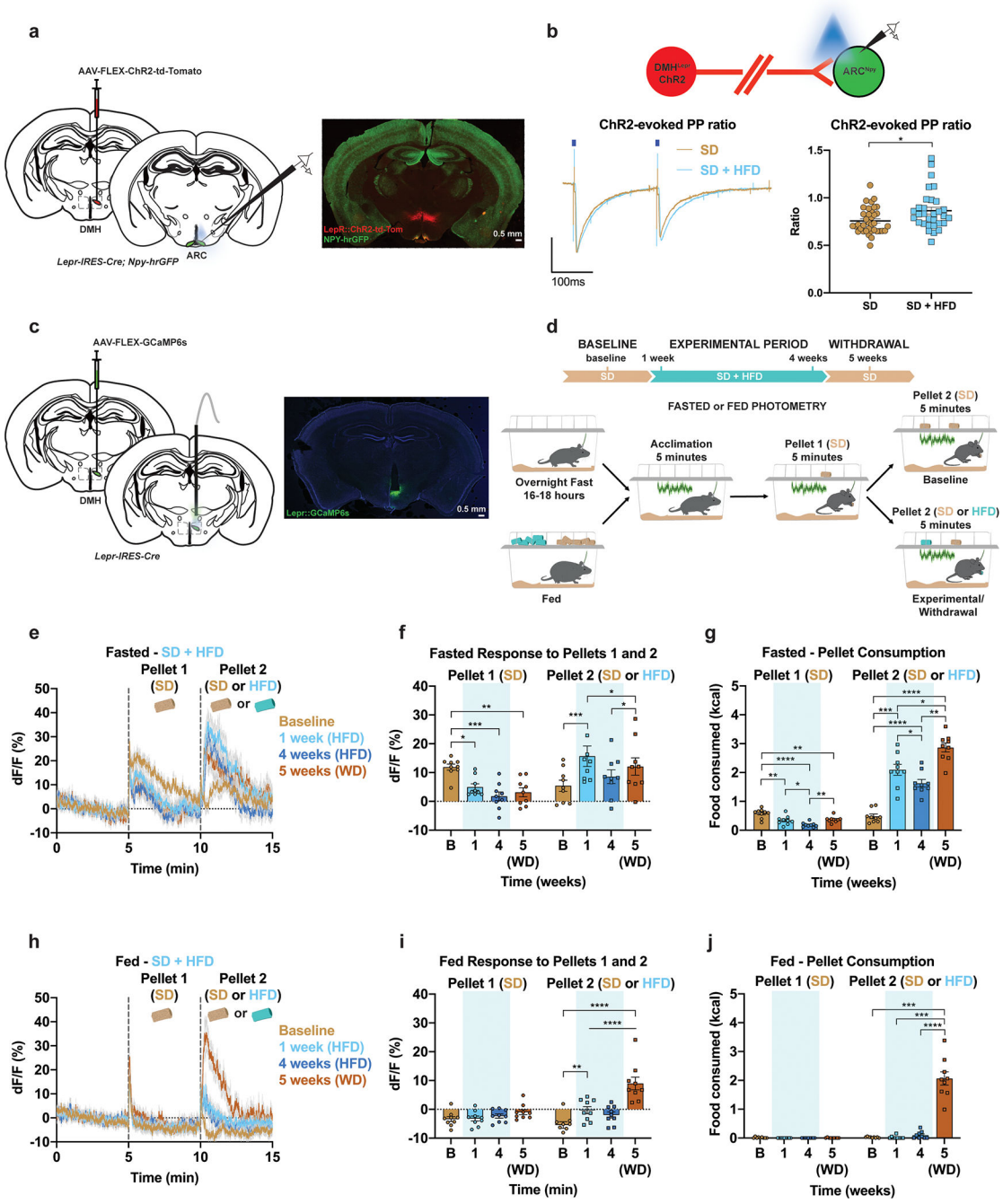

Figure 3: HFD exposure induces alterations in DMH^{LepR} responses to SD.

a, Left, Brain schematic of unilateral viral delivery of Cre-inducible ChR2 to the DMH of LepR-ires-Cre; Npy-hrGFP mice and position of ex vivo slice recordings from ARC^{Npy} cells. Right, representative image of ARC slice showing NPY-hrGFP and DMH^{LepR}::ChR2 terminals. **b,** Top, Schematic of light-evoked paired-pulse recordings. Left, representative traces. Right, quantification of ratio (n=37 cells/4 mice in the SD group, 31 cells/4 mice in the SD + HFD group, Unpaired t-test (two-tailed) Welch's correction, P=0.0152). **c,** Left, Brain schematic of unilateral viral delivery of Cre-inducible GCaMP6s to the DMH of

LepR-ires-Cre mice and optical fiber implant. Right, representative image of GCaMP6s expression. **d,** Experimental timeline and group schematic for both fasted and fed photometry recordings. **e,** Average fasted photometry traces across recording sessions aligned to Pellet 1 and 2 presentation (n=9, males and females). **f,** Within-subject quantification of fasted DMH^{LepR} activity response to Pellet 1 (SD) and Pellet 2 (SD at Baseline; HFD during 1, 4 and 5 weeks) (n=9, males and females, RM two-way ANOVA, Time x Pellet: F (3, 48) = 11.07, P<0.0001, Tukey's multiple comparisons) and **g,** total calories consumed across testing sessions (n=9, males and females, RM two-way ANOVA, Time x Pellet: F (3, 48) = 66.65, P<0.0001, Tukey's multiple comparisons). **h,** Average fed photometry traces across recording sessions aligned to Pellet 1 and 2 presentation (n=9, males and females). **i,** Within-subject quantification of fed DMH^{LepR} activity response to Pellet 1 (SD) and Pellet 2 (SD at Baseline; HFD during 1, 4 and 5 weeks) (n=9, males and females, RM two-way ANOVA, Time x Pellet: F (3, 48) = 14.44, P<0.0001, Tukey's multiple comparisons) and **j,** total calories consumed across testing sessions (n=9, males and females, RM two-way ANOVA, Time x Pellet: F (3, 48) = 81.11, P<0.0001, Tukey's multiple comparisons). Dotted lines in **e,h** indicate Pellet 1 and Pellet 2 presentation. Shaded blue area in **f-g**, and **i-j** represent HFD homecage availability. B refers to Baseline. WD=withdrawal. All error bars and shaded regions of **e-h** represent s.e.m. $*P < 0.05$, $**P < 0.01$, $***P < 0.001$, $****P < 0.0001$.

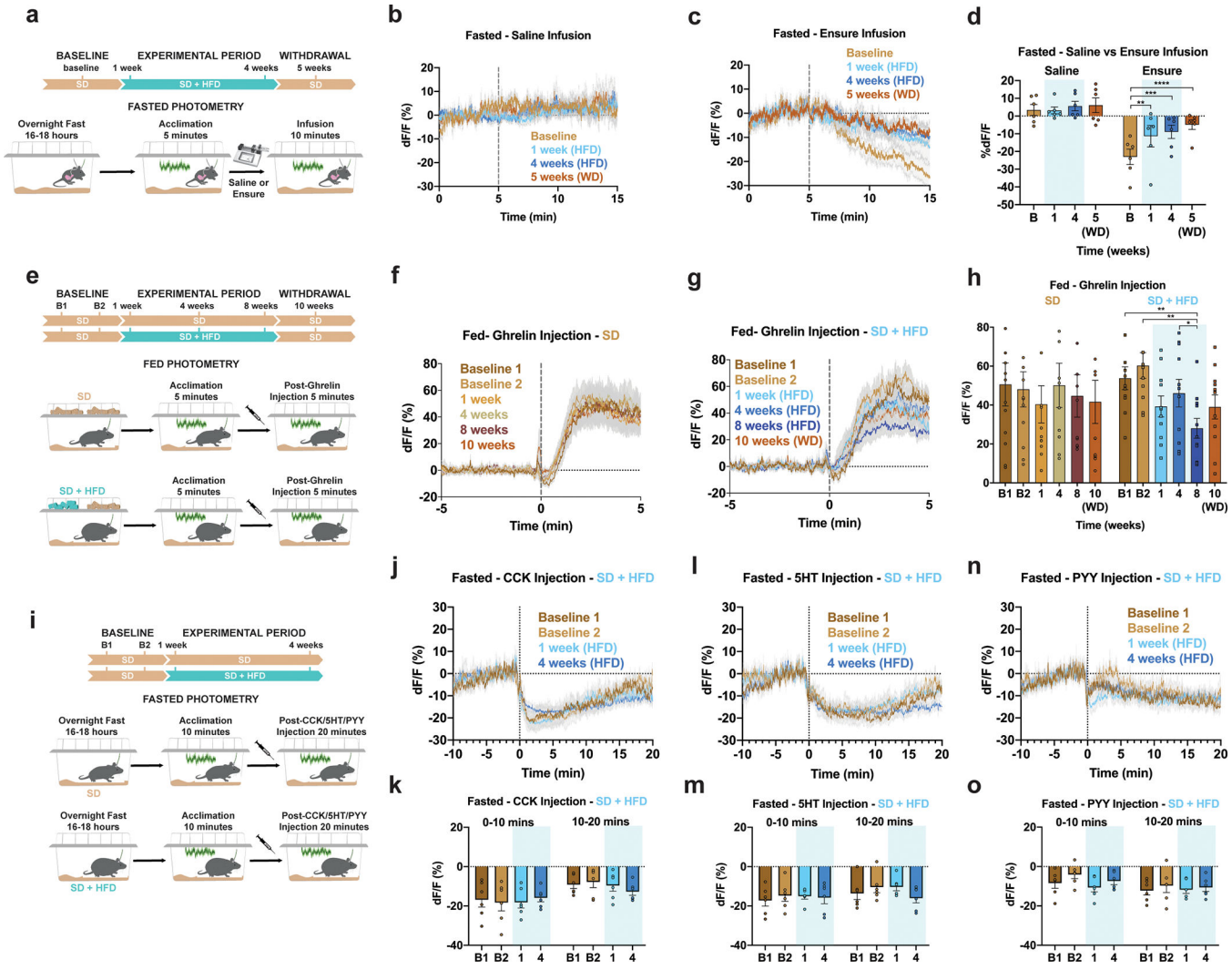

Figure 4: HFD-exposure disrupts ARC^{AgRP} responses to both peripheral detection of calories and signals of hunger.

a, Experimental timeline and group schematic for fasted photometry recordings during gastric infusions. **b-c,** Average fasted ARC^{AgRP} photometry traces in response to gastric infusion of **b,** saline or **c,** Ensure (n=6, males and females). **d,** Within-subject quantification of fasted ARC^{AgRP} activity response to gastric infusions of saline or Ensure across testing sessions (n=6, males and females, RM two-way ANOVA, Time x Infusion: F (3, 15) = 7.236, P=0.0032, Tukey's multiple comparisons). **e,** Experimental timeline and group schematic for fed photometry recordings during ghrelin injection. **f-g,** Average photometry traces of the **f,** SD group and **g,** SD + HFD group across recording sessions aligned to ghrelin injection (n=12 SD group, n=11 SD + HFD group, males and females). **h,** Within-subject quantification of ARC^{AgRP} activity to ghrelin across testing sessions (n=12 SD group, n=11 SD + HFD group, males and females, RM two-way ANOVA, Time x Group: F (5, 105) = 3.244, P=0.0092, Tukey's multiple comparisons). **i,** Experimental timeline and group schematic for fasted photometry recordings during CCK, 5HT or PYY injection. **j,l,n,** Average photometry traces of the SD + HFD group across recording sessions aligned to **j,**

CCK, **l,** 5HT or **n,** PYY injection (n=6 SD + HFD group, males and females). **k,m,o,** Within-subject quantification of ARC^{AgRP} activity to **k,** CCK (n=6 SD + HFD group, males and females, RM two-way ANOVA, Time bin x Week: F (1.681, 8.404) = 3.230, P=0.0961), **m,** 5HT (n=6 SD + HFD group, males and females, RM two-way ANOVA, Time bin x Week: F (1.656, 8.279) = 2.904, P=0.1158) or **o,** PYY (n=6 SD + HFD group, males and females, RM two-way ANOVA, Time bin x Week: F (2.081, 10.40) = 2.203, P=0.1583) across testing sessions. Dotted lines indicate **b-c,** infusion, **f-g,** ghrelin, **j,** CCK, **l,** 5HT or **n,** PYY injection. Shaded blue area in **d,h,k,m** and **o** represent HFD homecage availability. B1 and B2 refer to Baseline 1 and 2, respectively. WD=withdrawal. All error bars and shaded regions of **b-c, f-g, j, l,** and **n** represent s.e.m. $*P < 0.05$, $**P < 0.01$, $***P < 0.001$, $****P < 0.0001$.

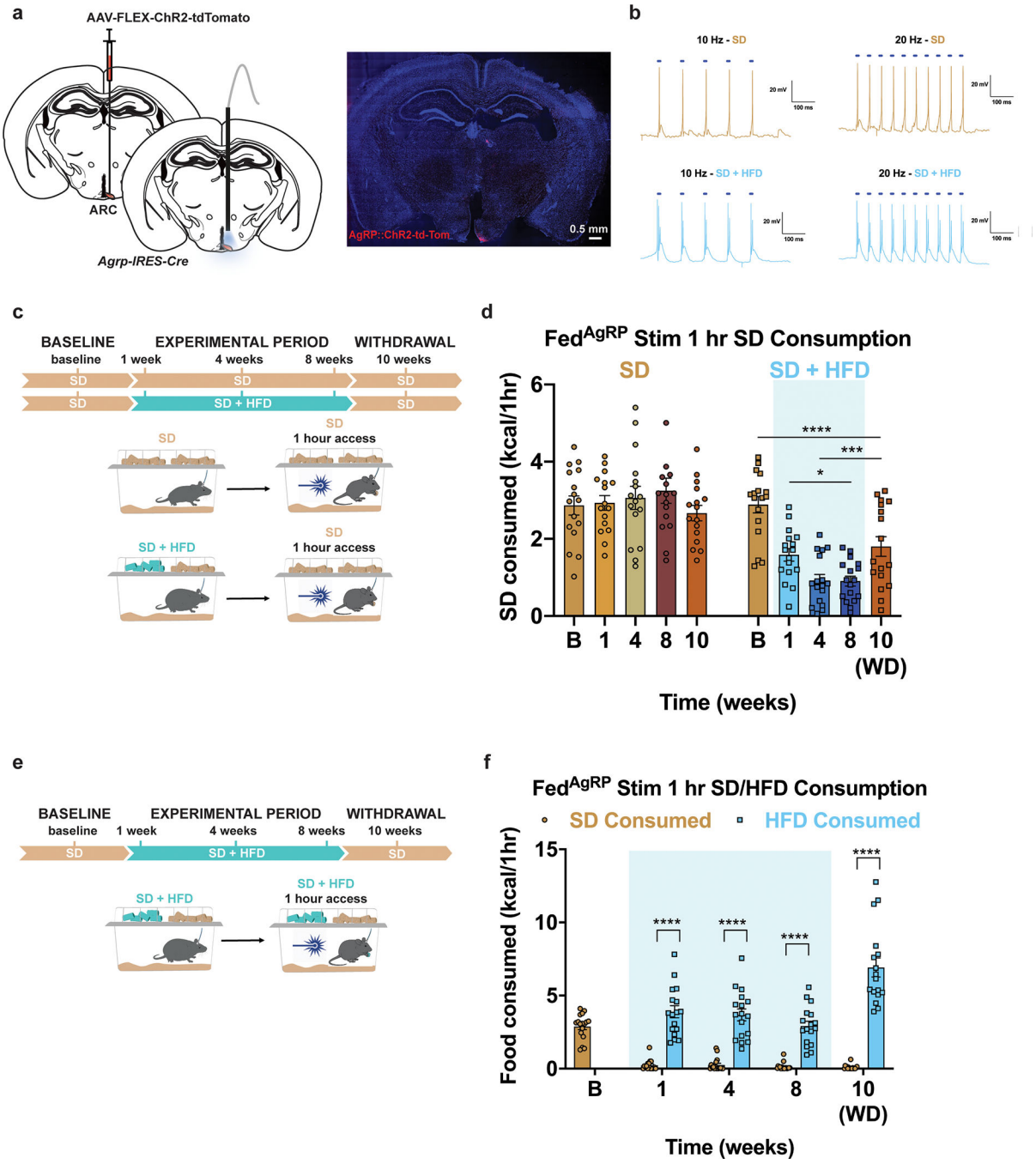

Figure 5: HFD-exposure disrupts functional capacity of ARC^{AgRP} neurons to drive SD, but not HFD, consumption.

a, Left, Brain schematic of unilateral viral delivery of Cre-inducible ChR2-tdTomato to the ARC of AgRP-ires-Cre mice and optical fiber implant. Right, representative image of ChR2-tdTomato expression. **b,** Light-evoked action potentials in AgRP::ChR2 mice in SD (top) and SD + HFD (bottom) groups. **c,** Experimental timeline and group schematic for optogenetic studies with 1 hr SD access. **d,** Within-subject comparison of fed^{AgRP} stimulation 1 hr SD consumption across testing sessions (n=16 SD group, n=17 SD + HFD

group, males and females, RM two-way ANOVA, Time x Group: F (4, 124) = 18.85, P<0.0001, Tukey's multiple comparisons). **e,** Experimental timeline and group schematic for optogenetic studies with 1 hr SD and HFD access. **f,** Within-subject comparison of Fed^{AgRP} stimulation 1 hr SD and HFD consumption across testing sessions (n=17, males and females, RM two-way ANOVA, Time x Diet: F (3, 96) = 26.03, P<0.0001, Bonferroni's multiple comparisons). Shaded blue area in **d** and **f** represent HFD homecage availability. B=Baseline. WD=Withdrawal. All error bars represent s.e.m. $*P < 0.05$, $**P < 0.01$, $***P < 0.001$, $****P < 0.0001$.

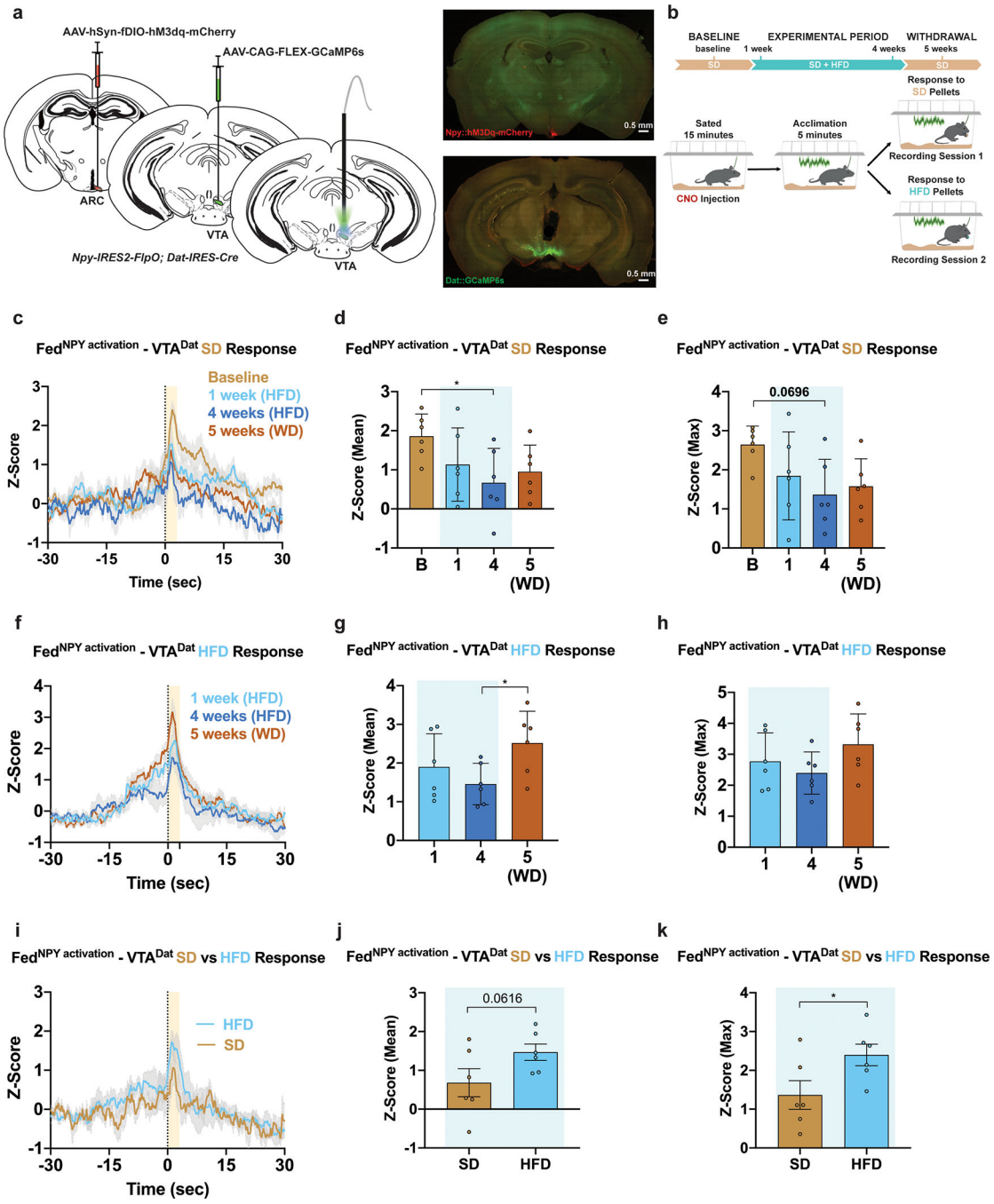

Figure 6: HFD alters ARC^{Npy}-mediated VTA^{Dat} responses to SD.

a, Left, Brain schematic of unilateral viral delivery of Flp-inducible hM3Dq and Cre-inducible GCaMP6s to the ARC and VTA, respectively, of Npy-ires2-FlpO; Dat-ires-Cre mice and optical fiber implant. Right, representative image of Npy::hM3dq (top) and Dat::GCaMP6s (bottom) expression. **b,** Experimental timeline and group schematic for fed photometry recordings. **c,f** Averaged Z-score traces of VTA^{Dat} activity aligned to **c,** SD or **f,** HFD pellet consumption across recording weeks. **d-e, g-h** Within-subject comparisons of **d,g** mean and **e,h** maximum fluorescence Z-score during **d,e,** SD (n=6, males and females,

RM one-way ANOVA, Time: F (3, 15) = 3.538, P=0.0407, Time: F (3, 15) = 2.802, P=0.0757, Tukey's multiple comparisons) or **g,h,** HFD pellet consumption across sessions (n=6, males and females, RM one-way ANOVA, Time: F (2, 10) = 4.073, P=0.0508, Time: F (2, 10) = 2.454, P=0.1358, Tukey's multiple comparisons). **i,** Comparison of averaged Z-score traces of VTA^{Dat} activity aligned to SD or HFD pellet consumption at 4 weeks. **j-k,** Within-subject comparisons of **j,** mean (n=6, males and females, Paired t test (two-tailed), P=0.0616) and **k,** maximum fluorescence Z-score comparing SD and HFD pellet consumption at 4 weeks (n=6, males and females, Paired t test (two-tailed), P=0.042). B=Baseline. WD=Withdrawal. Shaded peach region in **c,f** and **i** represent quantified pellet retrieval period. Shaded blue area in **d,e,g,h,j** and **k** represent HFD homecage availability. Time 0 denotes consumption. All error bars and shaded regions of **c,f** and **i** represent s.e.m. $*P < 0.05$.

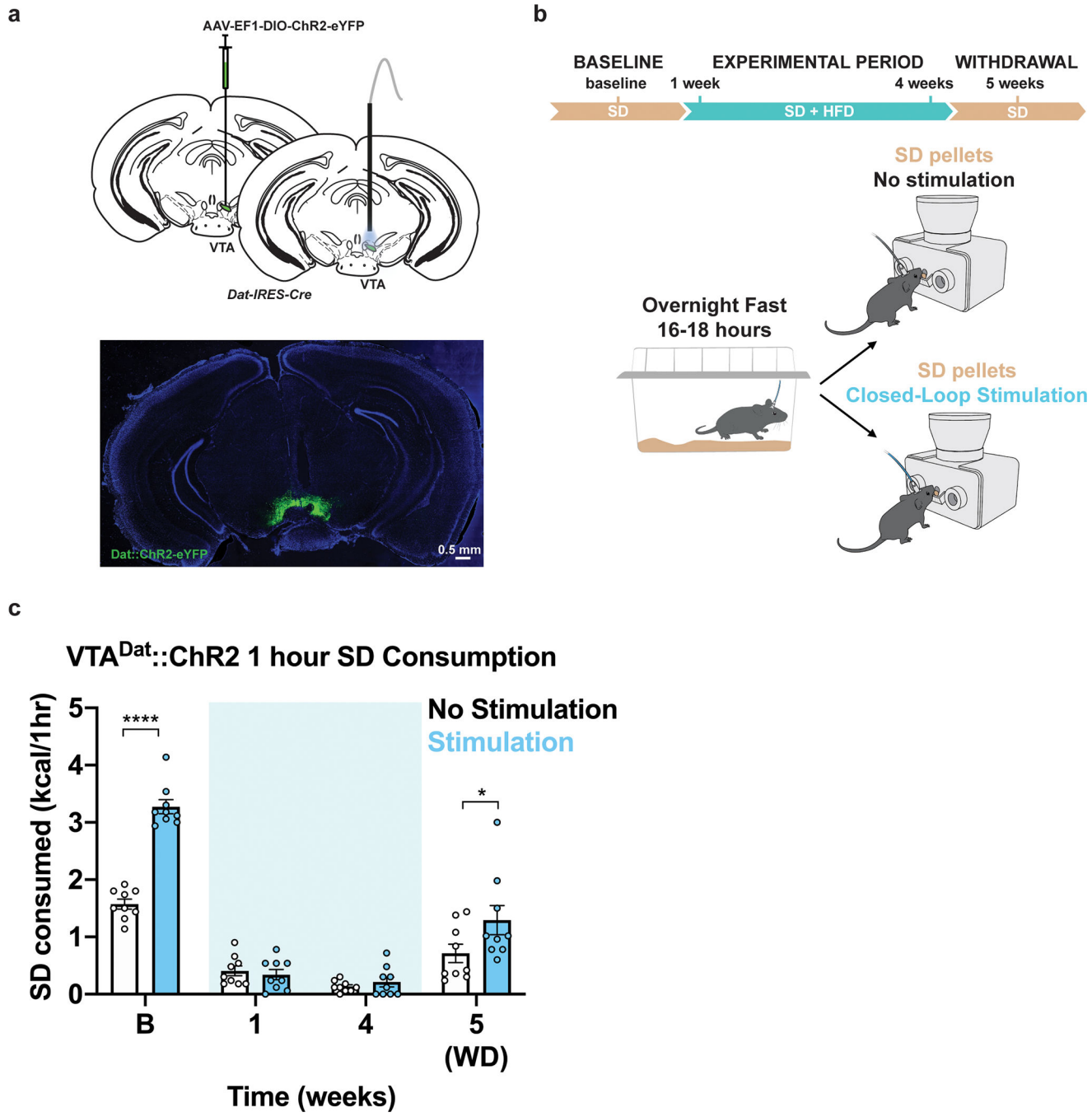

Figure 7: HFD-exposure disrupts functional capacity of VTA^{Dat} neurons to potentiate SD consumption.

a, Left, Brain schematic of unilateral viral delivery of Cre-inducible ChR2-eYFP to the VTA of Dat-ires-Cre mice and optical fiber implant. Right, representative image of ChR2-eYFP expression. **b,** Experimental timeline and group schematic for closed loop optogenetic studies with or without light stimulation. **c,** Within-subject comparison of 1 hr SD consumption across testing sessions with or without VTA^{Dat} photostimulation (n=9, males, RM two-way ANOVA, Time x Condition: $F(3, 48) = 18.30$, $P<0.0001$, Bonferroni's

multiple comparisons test). B=Baseline. WD=Withdrawal. Shaded blue area in **c** represents HFD homecage availability. All error bars represent s.e.m. *$P < 0.05$, ****$P < 0.0001$.

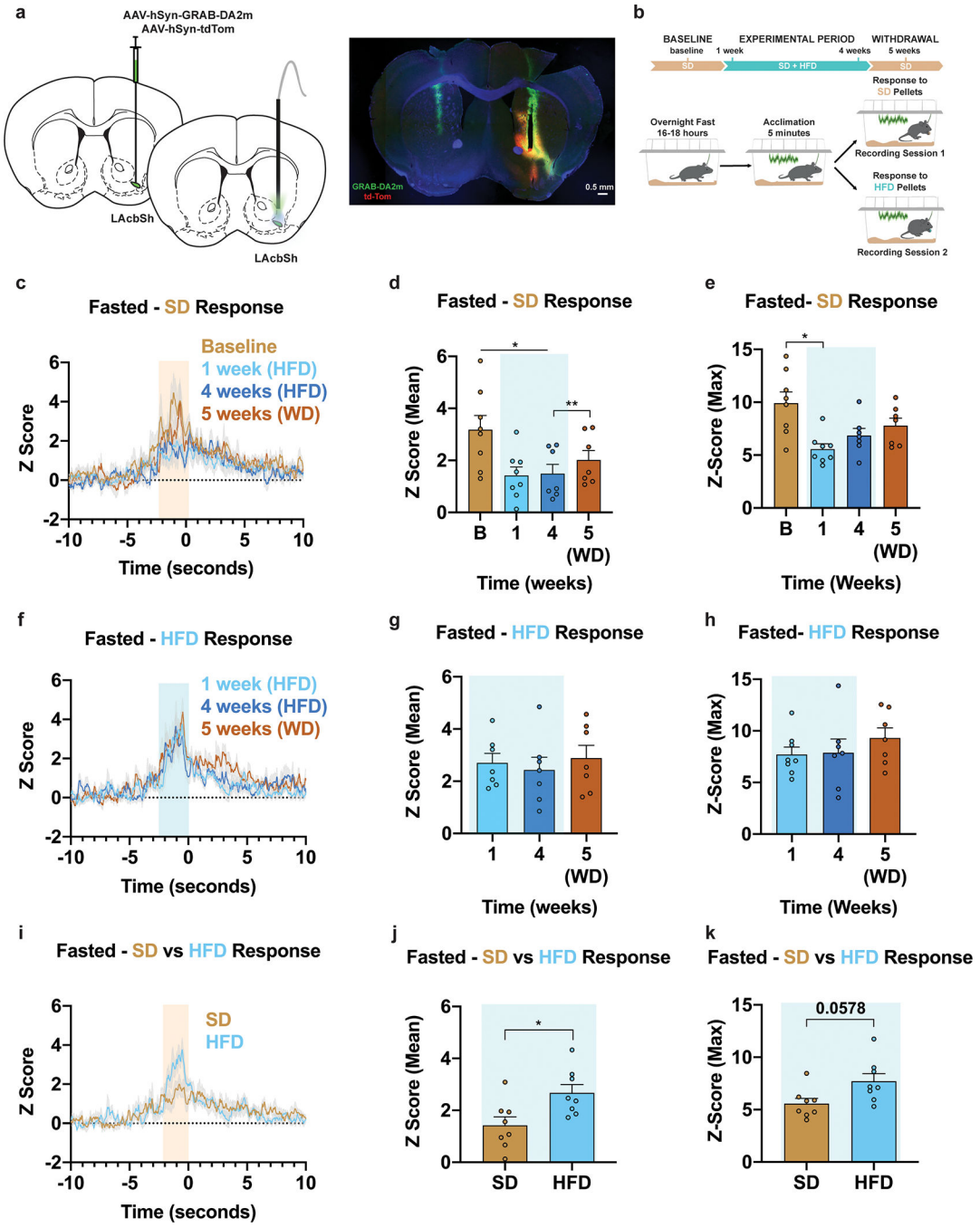

Figure 8: HFD-exposure dampens nucleus accumbens shell DA release in response to SD

a, Left, Brain schematic of unilateral viral delivery of the DA sensor GRAB-DA2m and tdTomato to the AcbSh and optical fiber implant. Right, representative image of Right, representative image of GRAB-DA2m and tdTomato expression in the AcbSh. **b,** Experimental timeline and group schematic for photometry recordings. **c,f** Averaged Z-score traces of DA2m fluorescence aligned to **c,** SD or **f,** HFD pellet retrieval across recording weeks. **d-e, g-h** Within-subject comparisons of **d,g** mean and **e,h** maximum fluorescence Z-score during **d,e,** SD (n=7–8, males and females, Mixed-effects model (REML), Time: F

(1.555, 9.847) = 11.91, P=0.0034, Time: F (1.599, 10.12) = 6.608, P=0.0182, Tukey's multiple comparison) or **g,h,** HFD pellet consumption across sessions (n=7–8, males and females, Mixed-effects model (REML), Time: F (1.950, 11.70) = 0.2897, P=0.7484, Time: F (1.832, 10.99) = 0.8452, P=0.4461). **i,** Comparison of averaged Z-score traces of DA2m fluorescence aligned to SD or HFD pellet consumption at 1 week. **j-k,** Within-subject comparisons of **j,** mean (n=8, males and females, Paired t test (two-tailed), P=0.021) and **k,** maximum fluorescence Z-score comparing SD and HFD pellet consumption at 1 week (n=8, males and females, Paired t test (two-tailed), P=0.0578). Shaded peach/blue region in **c,f** and **i** represent quantified pellet approach/retrieval period. Shaded blue area in **d,e,g,h,j** and **k** represent HFD homecage availability. B=Baseline. WD=Withdrawal. Time 0 denotes consumption. All error bars and shaded regions of **c,f** and **i** represent s.e.m. $*P < 0.05$, $**P < 0.01$.